JOURNAL OF GLACIOLOGY

CAMBRIDGE UNIVERSITY PRESS

Interactions between glacier dynamics, ice structure, and climate at Fjallsjökull, south-east Iceland

Journal:	*Journal of Glaciology*
Manuscript ID	JOG-18-0135
Manuscript Type:	Article
Date Submitted by the Author:	20-Nov-2018
Complete List of Authors:	Dell, Rebecca; University of Cambridge Scott Polar Research Institute, Department of Geography Carr, Rachel; University of Newcastle, Schoolof Geography, Politics and Sociology Phillips, Emrys; British Geological Survey, The Lyell Centre Russell, Andrew; Newcastle University, School of Geography, Politics and Sociology
Keywords:	Glacier calving, Glacier flow, Glacier delineation, Structural glaciology, Ice velocity

Journal of Glaciology, Vol. 12, No. 3, 2016 1

Interactions between glacier dynamics, ice structure, and climate at Fjallsjökull, south-east Iceland

Rebecca DELL,[1] Rachel CARR,[2] Emrys PHILLIPS,[3] Andy RUSSELL [2]

[1] *Scott Polar Research Institute, Cambridge University, Lensfield Road, Cambridge, CB2 1ER*

[2] *School of Geography, Politics and Sociology, Newcastle University, Newcastle Upon Tyne, NE1 7RU*

[3] *British Geological Survey, The Lyell Centre, Research Avenue South, Edinburgh, EH14 4AP*

Correspondence: Rebecca Dell <rld46@cam.ac.uk>

ABSTRACT. Over recent decades, the number of lake-terminating outlet glaciers in Iceland has increased in line with climate warming. The mass balance changes of these lake-terminating outlet glaciers are sensitive to rising air temperatures, due to altered glacier dynamics and increased surface melt. This study aims to better understand the relationship between proglacial lake development, climate, glacier dynamics, and glacier structure at Fjallsjökull, a large, lake-terminating outlet glacier in south-east Iceland. We used satellite imagery to map glacier terminus position and lake extent between 1973 and 2016, and a combination of aerial and satellite imagery to map the structural architecture of the glacier's terminus in 1982, 1994, and 2011. The temporal evolution of ice surface velocities between 1990 and 2017 was calculated using feature tracking. Statistically significant increases in the rate of terminus retreat and lake expansion were identified in 2001, 2009, and 2011. Our surface velocity and structural data sets revealed the development of localised flow 'corridors' over time, which conveyed relatively faster flow towards the glacier's terminus. We attribute the overall changes in dynamics and structural architecture at Fjallsjökull to rising air temperatures, but argue that the spatial complexities are driven by glacier specific factors, such as basal topography.

INTRODUCTION AND AIMS

Icelandic glaciers and ice caps are highly sensitive to atmospheric warming, and since the late 20th century, the rate of mass loss from Iceland has, therefore, been substantial (Pálsson and others, 2012; Björnsson and others, 2013; AMAP, 2017). This relatively high sensitivity to variations in climate is due to Iceland's position in the North Atlantic Ocean: which places Iceland at the boundary of the polar and mid-latitude atmospheric circulation cells, converging warm and cold ocean currents, and directly in the path of cyclonic westerlies that are driven by the North Atlantic Oscillation (Björnsson and Pálsson, 2008; Pálsson and others, 2012; Björnsson and others, 2013). In particular, the warm Irminger Current, which travels from the south-western coast of Iceland to the northern coast of Iceland, contributes to Iceland's temperate maritime climate (Vilhjálmsson, 2002).

Iceland has six major ice-caps, which account for 90% of its permanent ice cover (Foresta and others, 2016). These ice-caps have lost 5.8± 0.7 Gt a^{-1} between 2010-11 and 2014-15, which equates to a sea level rise contribution of 0.016 ± 0.002 mm a^{-1} (Foresta and others, 2016). However, this rate of mass loss was 40 % lower relative to the previous 15 years, in part due to a year of anomalous positive mass balance for Vatnajökull, Iceland's largest ice-cap, in 2014-2015 (Foresta and others, 2016). Owing to its size, changes in the mass of Vatnajökull can dominate the mass balance signal of Iceland, and can contribute considerably to sea level rise.

Vatnajökull is situated in south-east Iceland, and its mass loss is thought to be exacerbated by the development of lake-terminating outlet glaciers, which can accelerate terminus retreat through calving activity (Schomacker, 2010). Here, the development of proglacial lakes is facilitated by the presence of marked over-deepenings that underlay numerous retreating Icelandic glaciers (Schomacker, 2010; Magnússon and others, 2012). Examples of lake-terminating outlet glaciers that drain the Vatnajökull Ice-Cap include Breiðamerkurjökull, Fjallsjökull, Skaftafellsjökull, Svínafellsjökull, Virkisjökull/Falljökull, Heinabergsjökull, Hoffellsjökull and Fláajökull. Nearly all of Vatnajökull's ice marginal lakes have expanded since 1995, and the size and number of these lakes is predicted to increase in the future due to climate warming (Flowers and others, 2005; Schomacker, 2010). For example, Jökulsárlón, Breidamerkurjökull's pro-glacial lake, expanded by 6 km^2 between 2000 and 2009 (Schomacker, 2010).

Lake-terminating outlet glaciers can lose mass through a number of additional mechanisms when compared to land-terminating glaciers. These additional mechanisms are influenced by interactions at the glacier-lake boundary, and include thermally induced melt, changes to the longitudinal stress regime, the formation of basal crevasses, and force imbalances at the terminus (Benn and others, 2007; Carrivick and Tweed, 2013). These mechanisms often result in calving events. The timing, nature, and magnitude of these calving events are controlled by a range of factors which are glacier specific (e.g. subglacial topography and glacier structures) and non-glacier specific (e.g. lake temperature) (Westrin, 2015).

An increase in the calving activity of a glacier can lead to the initiation of a number of positive feedbacks (Meier and Post, 1987; Van der Veen, 1996; Van der Veen, 2002; Vieli and others, 2002; Benn and others, 2007; Joughin and others, 2008; Carr and others, 2013; Hill and others, 2018). For example, it can cause the glacier to retreat into deeper water, which will increase the buoyant forces acting on the terminus, increase torque, and subsequently increase the rate of calving activity and associated retreat (Van der Veen, 1996; Van der Veen, 2002; Benn and others, 2007). In addition, a glacier terminus could begin to float as buoyant forces increase, this can reduce effective pressure at the ice-bed interface, and facilitate an increase in glacier velocities and longitudinal stretching (Van der Veen, 1996; Van der Veen, 2002; Benn and others, 2007). These changes may subsequently lead to thinning of the terminus, rendering it more vulnerable to fracturing and calving activity (Van der Veen, 1996; Van der Veen, 2002; Benn and others, 2007).

Proglacial lakes are becoming increasingly widespread globally (e.g. Iceland, Patagonia, New Zealand, and the Himalaya), and can strongly enhance ice loss (Motyka and others, 2003; Bolch and others, 2011; Dykes and others, 2011; Carrivick and Tweed, 2013). However, our understanding of the interactions between proglacial lakes and their adjacent glaciers are not fully understood (Benn and others, 2007; Carrivick and Tweed, 2013). This study therefore presents the results of a detailed analysis of the changing dynamic and structural regime of Fjallsjökull in response to variations in local climate between 1973 and 2017. Fjallsjökull was selected for this type of study as it terminates in the third largest proglacial lake associated with an outlet glacier draining the south-east Vatnajökull Ice-Cap. Furthermore, Fjallsjökull's proglacial lake has received minimal attention in scientific studies, with most work focusing on Breidamerkurjökull's proglacial lagoon, Jökulsárlón.

This study aims to better understand the relationship between proglacial lake development, local climate, glacier dynamics, and glacier structure at lake-terminating outlet glaciers. We use satellite imagery from various platforms to calculate the change in terminus position, lake area, surface velocities, and surface structures over time. From these data, we propose a conceptual model, which combines structural and

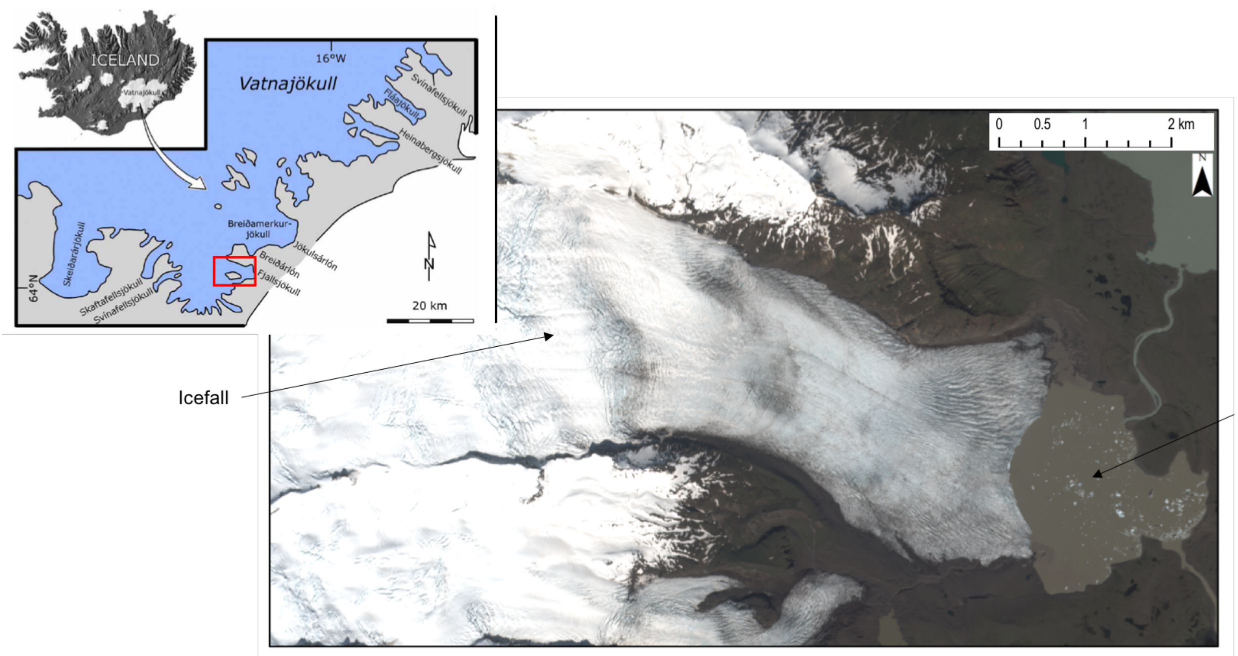

Fig. 1. A map of the study area, Fjallsjökull, in the context of Iceland and the south-east Vatnajökull ice-cap (subset). The red box indicates the extent of Fjallsjökull in the subset image. Subset image source: modified from Schomacker (2010). Satellite image source: Sentinel 2 image from the 6th June 2018 (downloaded from Earth Explorer).

velocity datasets, to explain the development of a distinctive 'concentrated' ice flow regime at Fjallsjökull.

METHODS

Study Area

Fjallsjökull is located on the eastern side of the Öræfajökull ice-cap, south-east Iceland (Evans and Twigg, 2002) (Figure 1). The Öræfajökull ice-cap occupies the caldera of Öræfajökull stratovolcano and is located on the southern side of the much larger Vatnajökull ice-cap (Magnússon and others, 2012, Phillips and others, 2017). Fjallsjökull descends from the south-eastern side of Öræfajökull, and is composed of a series of ice falls (Evans and Twigg, 2002) before terminating in a large (3.7 km^2 in 2016) proglacial lake, called Fjallsarlön (Figure 1). Fjallsarlön is located within a 3 km wide by 4 km long, c. 206 m deep overdeepening, which is being revealed in response to the westward lateral retreat of the margin of Fjallsjökull (Howarth and Price, 1969; Magnússon and others, 2012).

Optical Imagery

Twenty six remotely sensed optical images, including Landsat (downloaded from: https:// earthexplorer.usgs.gov), Sentinel 2 (downloaded from: https://earthexplorer.usgs.gov), Google Earth (downloaded from: the Google Earth Pro application), and National Land Survey of Iceland Imagery (http://www.lmi.is/wp-content/uploads/2013/10/L for-use-of-free-NLSI-data-General-Terms.pdf) were downloaded for the period between 1979 and 2017 (Table A.1). Imagery was downloaded if the area of interest was cloud free, and not obscured by scan line failures associated with the Landsat 7 ETM+ satellite. For the purpose of frontal position change and lake area change analysis, images were obtained for the summer months of July-September as these months had little snow cover, and regions could be mapped with greater accuracy (Table A.1 and Figure A.1). To be sure that we were not picking up a signal from seasonal variation by using imagery across these 3 months the terminus position was digitised from a July image (07/07/2015) and a September image (25/09/2015). The terminus position change between these two images was 9.9 m, which was within 0.1 of the minimum total error (geolocation error + digitisation error) associated with the Landsat 8 imagery. Images for structural mapping were obtained between June and August (Table A.1 and Figure A.5). Images for feature tracking were selected with a minimum temporal gap of 11 months, to resolve velocity changes (Table A.2). This time gap was determined by visually assessing the offset of features between images within image pairs.

Frontal Position Change and Lake Area Change

The rectilinear box method (e.g. Moon and Joughin, 2008; Lea and others, 2014) was used to calculate frontal position change for 13 time steps between 1973 and 2016. This method was selected as it can account for asymmetric changes at a calving front (e.g. Lea and others, 2014; Larsen and others, 2016). The width of the rectilinear box encompassed the maximum width of the lake-terminating portion of Fjallsjökull (identified in 2016), rather than the full width of the terminus. This approach minimised potential errors in accurately identifying the location of the land-terminating portion of Fjallsjökull, which is debris covered and is difficult to distinguish from its surroundings. This approach is further justified due to the study's focus on the impact of the lake on glacier dynamics and structural change.

Landsat 7 ETM and Landsat 8 OLI/TIRS images were pan sharpened using band 8, to produce a 15 m pixel resolution output in RGB. These images were then used to delineate the terminus position at a scale of 1:6,000. For the Landsat 1-5 MSS images (60 m pixel resolution) and Landsat 4-5 TM images (30 m pixel resolution), the terminus was digitised at scales of 1:12,500 and 1:10,000 respectively (Table

A.3). These scales allowed the accurate mapping of the terminus position and prevented images from becoming too pixelated for reliable interpretation (Lovell, 2016). To show that this approach did not affect the results, the terminus position for each satellite sensor type was digitised at the greatest spatial scale used (1:12,500). Under 0.25% variation was found in both the mean terminus length and lake area relative to the original measurements using different scales.

Frontal Position Change and Lake Area Change

Lake area change was quantified using the same imagery, time steps, and digitising scale as frontal position change. At each time step, the lake boundary was manually digitised. Channels exiting the lake were excluded from the shape-file at the point of inflection (i.e. where the channel began to form). In addition, the proportion of Fjallsjökull's margin that terminated in Fjallsarlön was calculated over the study period, by dividing the length of the glacier margin that terminated in the lake by the full terminus length.

Two error sources are present with frontal position and lake area change calculations: manual digitisation errors and co-registration errors (Table A.4). The former was quantified by digitising the terminus position/ lake area of Fjallsjökull for the different satellite image types, and calculating the mean difference in terminus position relative to the original measured value (Carr and others, 2014). The latter was quantified by assessing the offset of each satellite image type relative to a base scene. For the purpose of this study, a Landsat 8 image was selected as the base scene, as the Landsat 8 images used had low geolocation errors (7.8-8.9 m Root Mean Square Error (RMSE)) and scenes from this sensor were used throughout the study (Table A.4).

Ice Surface Elevation Change

Changes in ice surface elevation were investigated using the Arctic DEM dataset which is available from the Polar Geospatial Centre (https://www.pgc.umn.edu/data/arcticdem). This dataset provides digital surface models (DSMs) for areas north of 60° from 2011 in some regions (Morin and others, 2016). The Arctic DEM data has a spatial resolution of 2 m, and are typically downloaded as 17 km by 110 km strips (Barr and others, 2018). However, at Fjallsjökull, few data strips covered the full region of interest, and data availability was therefore limited to 2012 and 2013. Once the DSMs were downloaded, they were co-registered using the ArcticDEM toolbox in ArcGIS and changes in ice surface height between 2012 and 2013 were calculated using the minus tool in the ArcGIS geoprocessing toolbox.

Near-terminus Velocities

Surface velocities at Fjallsjökull were calculated in the open-source feature tracking toolbox 'Image Geo-Rectification and Feature Tracking' (ImGRAFT) (http://imgraft.glaciology.net) using MATLAB (Messerli and Grinsted, 2015). Pre-processing steps included clipping all images to the same extent, to reduce the total processing time. In an attempt to increase the surface texture of the input images and increase the number of displacement retrievals (Fahnestock and others, 2015), a high pass filter was tested on images. However, it was found that this approach led to an increase in the number of false-positive retrievals for the flow orientation, and this step was, therefore, disregarded. False-positive retrievals of the flow orientation were identified as the ice flow direction was orientated up-glacier, against the glacier's gravity driven flow, which is highly unlikely to occur over large areas, due to the steep topography. Errors associated with the surface velocity calculations were quantified by taking the mean of five displacement values for stationary features (e.g. valley sides and arêtes) within each image pair (cf. Lea and others, 2014). The average surface velocity error across all image pairs was 7 m a^{-1} (Table A.5).

Within ImGraft there are a series of processing parameters that can be changed including: template size (60 x 60); search image size (100 x 100); regular gridded points (5 x 5); and the signal to noise ratio (0.6) (Messerli and Grinsted, 2015). In this study these parameters were systematically adjusted to find the flow field that best fitted the following two criteria: (i) to minimise the number of flow directions orientated up-glacier, and (ii) minimise any extremely high values. Currently, there are no direct measurements or InSAR data of surface velocities at Fjallsjökull, and therefore it was not possible to compare the feature tracking results against pre-existing datasets. The majority of time steps assessed were for one year, but due to image availability, the data set included one three-year step (1991-1994), which was subsequently converted to mean annual velocities.

Glaciological Structures

Following the methodology outlined by Phillips and others (2017) three detailed structural maps of Fjallsjökull's terminus were created for 1982, 1994, and 2011. These time steps were selected based on image availability, and because they provide an insight into the glacier's structural evolution on decadal timescales. Surface fractures were mapped at a scale of 1:500 for 1982 and 1994, and at a scale of 1:1000 in 2011. These scales were selected based on the resolution of the base images (Table A.3). The 2011 structural map provides a comprehensive overview of the most recent structural regime at Fjallsjökull, and extends 2.5 km up-glacier, whereas the 1982 and 1994 structural maps extend 0.75 km up-glacier, focusing on the structural development of the calving front. This approach allowed us to assess the glacier's wider structural composition in near-present day (2011). Fractures were grouped into domains based on variations in fracture orientation following Phillips and others (2017). The orientation (strike) of the fractures was calculated using a Python script within ArcGIS (Diaz Doce, 2014, unpublished) and the data plotted as a series of rose diagrams using the software package Stereostat by Rockworks TM.

Meteorological Data

Meteorological data were downloaded from the Icelandic Meteorological Office (http://en.vedur.is/climatology/data/) for 1973 to 2016. Daily air temperature data were obtained from two stations, Kvísker and Fagurhólsmýri, due to their close proximity to Fjallsjökull. Data were available from 1973 to April 2008 at Fagurhólsmýri, and from May 2008 to present at Kvísker. The measurements from these two stations were combined to produce a full time series of mean annual air temperatures over the study period (1973 to 2016). These data were used to calculate mean annual air temperatures, mean summer air temperatures (for June-August), and annual positive degree day (PDD) sums. To minimise the introduction of bias through missing values, years that were missing a month of data (2008 and 2010), and months that had less than 22 days of data, were excluded from further analysis (Carr and others, 2013). Subsequently, mean summer air temperatures were calculated from the daily data for June, July and August. Annual PDD sums were calculated from the sum of the daily temperatures that were above 0°C for each year. Total annual precipitation data for 1973 to 2011 was downloaded from the Icelandic Meteorological Station at Kvísker.

Statistical Analysis

'Change-point' analysis was conducted to test for statistically significant breaks in the terminus position data, lake area data, and meteorological data (Eckley and others, 2011; Killick and others, 2012; Carr and others, 2017). This analysis was performed in MATLAB using the 'findchangepts' function, following Hill and others (2018). The function used linear regression to identify significant breaks in each of the time series. Up to three change-points were searched for within each of the datasets, with the most significant breaks in the data being identified as change-points.

Table 1. The statistically significant change-points identified for terminus position and lake area over the study period.

	Change-Point(s)
Terminus Position	2001, 2009, 2011
Lake Area	2001, 2009, 2011

RESULTS

Terminus Position and Lake Area

The margin of Fjallsjökull retreated by 1.21 km between 1973 and 2016 (Figure 2). Between 1973 to 1991 and 1994 to 1998 there was no discernible change in ice margin position. These periods were separated by a small (0.09 km) phase of retreat between 1991 and 1994 (Figure 2). However, since 1998 the rate of ice margin retreat increased substantially and this higher rate was sustained for the remainder of the study period with a mean annual rate of 0.055 km a^{-1} (Figure 2). Coincident with terminus retreat, lake area increased by 2.72 km^2 between 1973 and 2016 (Figure 2). In 1973 to 1991 and 1994 to 1998 there was no discernible increase in lake area, separated by a 0.17 km^2 increase in area in 1991 to 1994 (Figure 2). Since 1994, however, lake area increased by 2.42 km^2. Importantly, the accelerated rate of terminus retreat in 2011 to 2016 (0.06 km a^{-1}) coincided with a period of relatively fast lake expansion (0.15 km^2 a^{-1}) (Figure 2), and change-point analysis identified comparable changes in the terminus position and lake area data sets, in 2001, 2009, and 2011 respectively (Table 1).

Ice Surface Elevation Change

Between 2012 and 2013, Fjallsjökull underwent ice surface elevation changes ranging from 43.6 m to 33.8 m (Figure 3). Within 1.2 km of the calving front, a widespread thinning trend was observed, with the magnitude of thinning ranging from c. - 4 m towards the glacier's lateral margins to c. -10 m towards the glaciers central axis (Figure 3). Thinning was recorded up to 3 km up-glacier of the calving front, with the magnitude of thinning gradually decreasing to c. 1 m as the distance up glacier increased. Above 3 km, the glacier's ice surface elevation predominantly increased by c. 1-2 m (Figure 3).

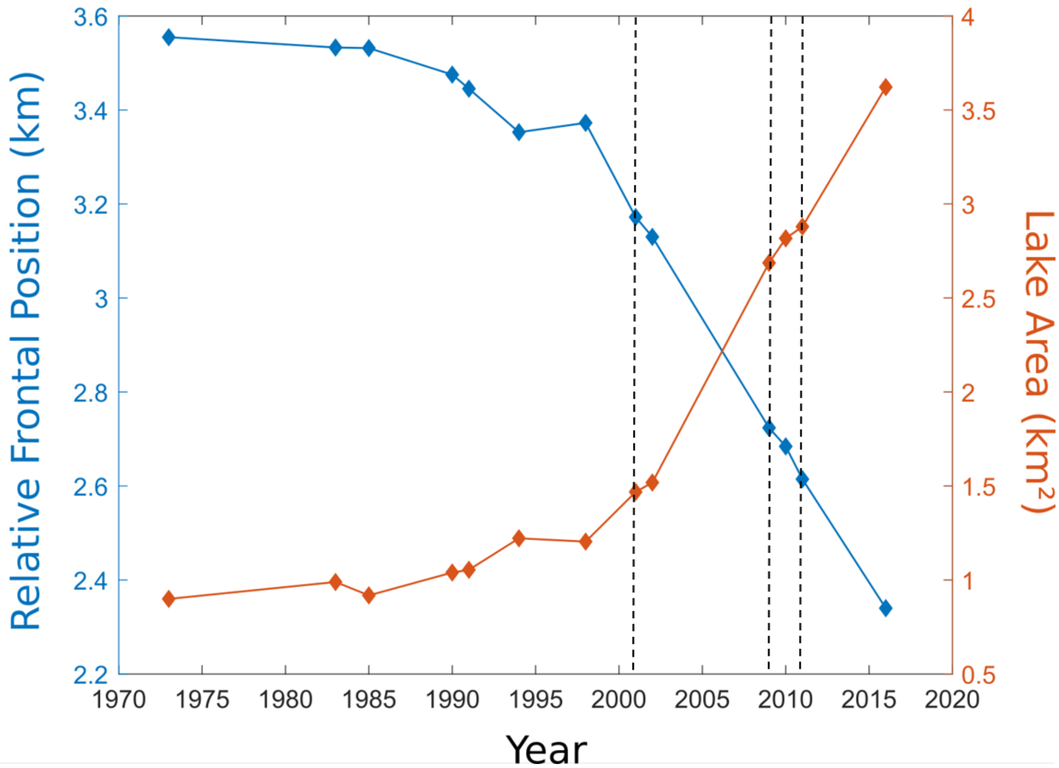

Fig. 2. Lake area and relative frontal position between 1973 and 2016. The vertical dashed lines indicate where statistically significant change-points were identified for both data sets.

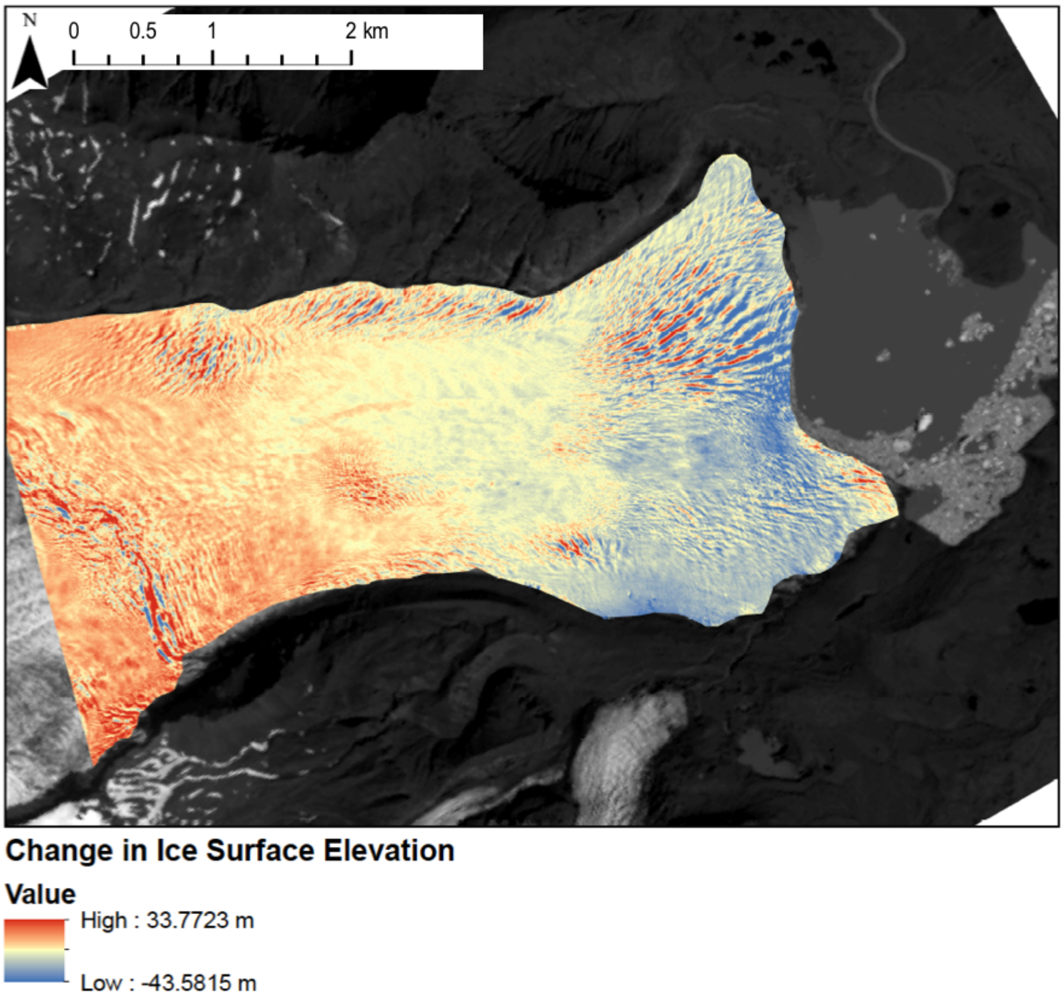

Fig. 3. Change in ice surface elevation at Fjallsjökull between 2012 and 2013, calculated using Arctic DEM digital surface models.

Table 2. A list of the meteorological variables investigated and the identified statistically significant change-point(s) identified over the study period.

Meteorological Variable	Change-Point(s)
Atmospheric Air Temperatures	1979, 1992
Summer Air Temperatures	2015
Positive Degree Days (PDD)	1984, 2013
Precipitation	1989, 2002, 2010

Climatic Trends

Overall, mean annual surface air temperatures and mean summer surface air temperatures increased by 2.1 °C and 1.5 °C respectively between 1973 and 2016 (Figure 4). Mean summer air temperatures were greatest in 2003 (11.1 °C), 2014 (11.2 °C), and 2016 (10.9 °C). The mean annual PDD sum increased by 511.3 between 1973 and 2011, and peaked in 2014 at 2437.7 (Figure 4). Change-points were identified in 1979 and 1992 for mean annual surface air temperatures, in 1984 and 2001 for PDD, and in 2015 for mean summer surface air temperatures (Table 2). Total precipitation increased by 999.4 mm between 1973 and 2011 at the Kvísker weather station. Peaks in total precipitation occurred in 2002 (4630.3 mm), 2006 (4477.7 mm), and 2011 (4556.6 mm) (Figure 3). Change-points in the precipitation data were identified in 1989, 2002, and 2010 (Table 2).

Glacier Surface Velocities

We observed marked increases in the average values and spatial complexity of glacier surface velocities in the period between 1990 and 2017 (Figure 5). In 1990-1991, surface flow was slow, and the flow directions were arranged in a radial fan-like pattern (Figure 5a), typically equated with a plug-flow style of glacier movement as the ice spreads laterally to form a piedmont lobe. Towards the glacier's centre line, velocities ranged between 20 and 40 m a^{-1} (Figure 5a). The magnitude, orientation, and patterns of surface velocities at Fjallsjökull changed little between 1990-1991 and 1991-1994 (Figures 5a and 5b).

However, between 1991-1994 and 2000-2001, there was a substantial increase in the spatial complexity and magnitude of surface velocities, as a pulse of relatively fast flowing ice migrated towards the margin of the glacier. Region 'i' indicates the origin of this pulse, a newly formed area of WNW-ESE trending

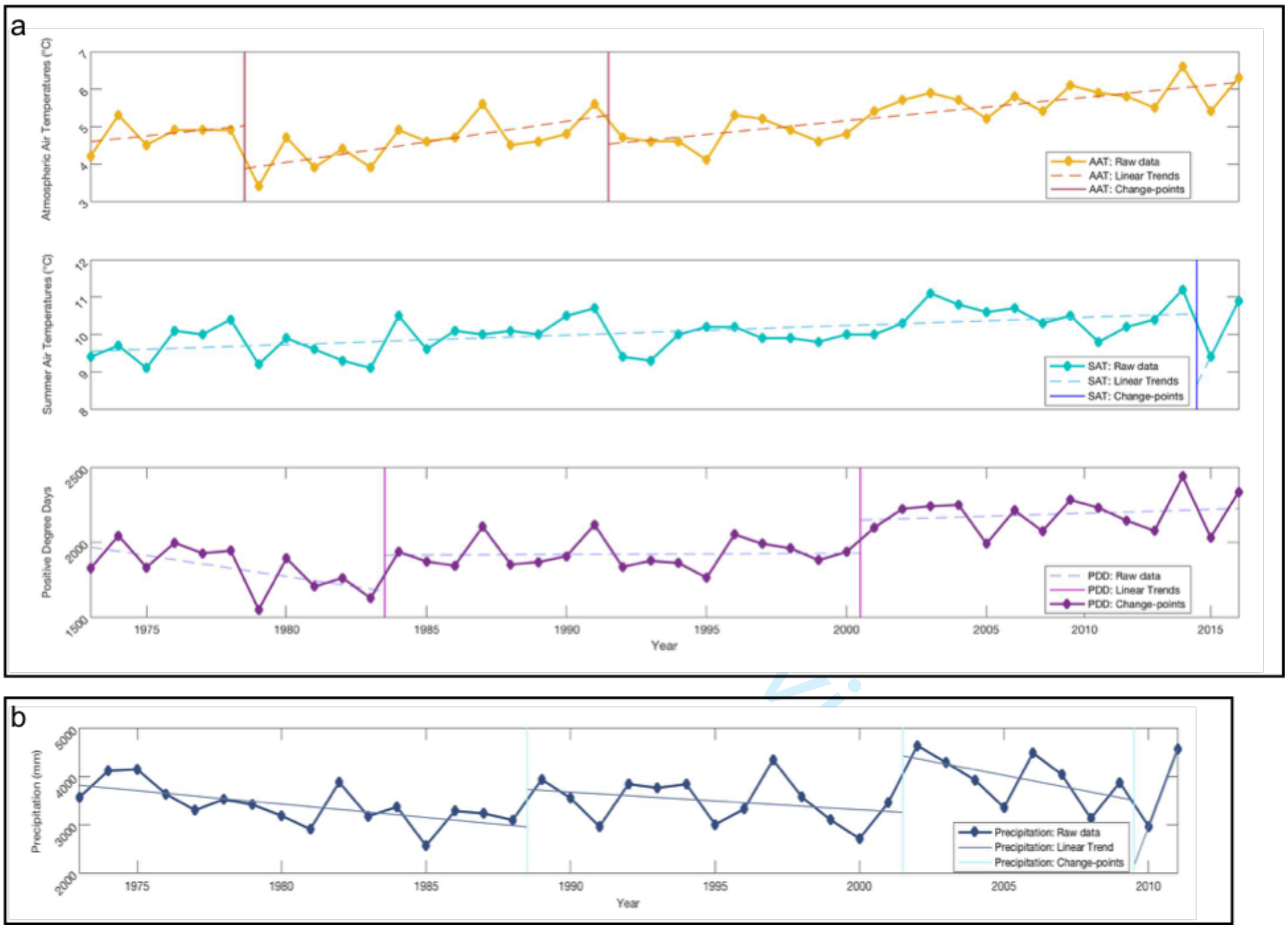

Fig. 4. Climate data: (a) shows mean annual air temperatures, mean summer air temperatures, and positive degree days between 1973 and 2016, (b) shows total annual precipitation between 1973 and 2011.

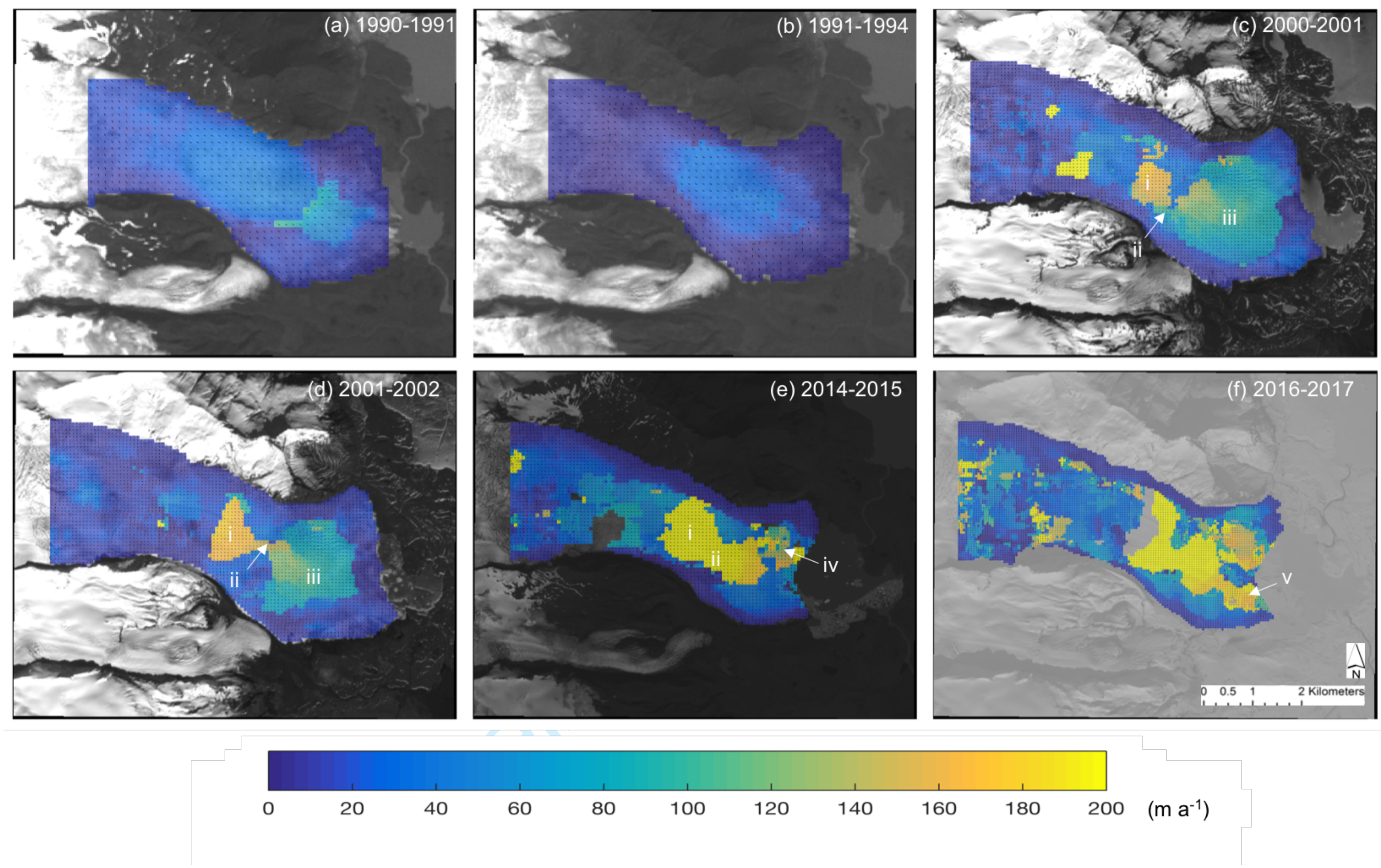

Fig. 5. Surface velocities at Fjallsjökull's terminus between 1990 and 2017. Labels i-v indicate notable features within the surface flow velocity fields. 'i' marks a distinct patch of relatively faster flow, 'ii' marks a 'corridor' of ice flow, 'iii' marks a laterally and longitudinally extensive area of relatively faster flow velocities, 'iv' marks a northern 'corridor' of relatively faster flow towards the margin, and 'v' marks a southern 'corridor' of relatively faster flow towards the glacier margin. Values presented in (b) represent mean annual average flow speeds. Sub-images 19a and 19b are based on calculations from Landsat 4-5 TM images, sub-images 19c and 19d are based on calculations from Landsat 7 ETM + images, sub-image 19e is based on calculations from Landsat 8 OLI/TIRS images, and sub-image 19f is based on calculations from Sentinel-2 MSI images.

relatively fast flow (170 m a^{-1}) (Figure 5c). This ice then migrated down-ice through region 'ii' (a narrower region of relatively faster flow velocities), and eventually into region 'iii' (a 2 x 2.3 km region of faster flow located adjacent to the glacier margin) (Figure 5c). Within region 'iii', velocities were much greater in the northwest (140 m a^{-1}) relative to the northeast (80 m a^{-1}) (Figure 5c). External to these regions, velocities ranged between 0 and 40 m a^{-1} (Figure 5c). Between 2000-2001 and 2001-2002, region 'i' (the origin of the relatively fast flowing pulse) had extended further, and covered 1.5 km of the terminus' width (Figure 5d). In addition, region 'ii', which acted as a 'corridor' for the fast flow velocities had migrated to a more central position, and calculated velocities were as great as 160 m a^{-1} (Figure 5d).

By 2014-2015, the relative surface velocities had further increased in magnitude and spatial complexity. Velocities in the origin region 'i' increased further, and peaked at 200 m a^{-1} (Figure 5e), and region 'ii' widened by 800 m. In addition, a fast flow corridor developed in the northern portion of the terminus (region 'iv') which connected region 'iii' to the calving front, and exhibited flow speeds between 100 and 200 m a^{-1} (Figure 5e). Outside of the fast flowing regions, ice velocities at the land-terminating sections of the glacier were between 0 and 10 m a^{-1}, and between 40 and 60 m a^{-1} at the lake-terminating portions (Figure 5e). From 2014-2015 and 2016-2017, velocities in region 'iv' increased. Furthermore, a new corridor of fast flow developed (region 'v') in the southern section of Fjallsjökull's terminus, trending in a WNW-ESE direction, with velocities between 110 and 200 m a^{-1} (Figure 5f). Flow between these fast flow corridors was relatively slow, ranging from 20 to 100 m a^{-1} (Figure 5f).

Overall, Fjallsjökull's surface flow regime became increasingly complex between 1990 and 2017 (Figure 6). Early data (1990-1994) show relatively slow flow velocities (0-30 m a^{-1}) at the glacier's margin and moderate flow velocities (30-110 m a^{-1}) towards the glacier's central axis (Figure 6). Flow directions were arranged in a splaying pattern and flow directions within the glacier's central zone were directed towards the calving front (Figure 6). In contrast, by 2016-2017, fast flow ($\geqslant$ 110 m a^{-1}) dominated the central portions of the terminus, and pulsed towards the glacier margin through two fast flow 'corridors', which extended from approximately 2.6 km inland to the calving front (Figure 6). At the outer margins of the fast flow 'corridors' medium flow velocities typically dominated, orientated in the direction of the calving front (Figure 6). However, with increasing distance from the fast flow 'corridors' and increasing proximity towards the glacier's lateral margins, there was a gradational reduction in flow velocities and change in flow orientation (Figure 6). The glacier's lateral margins continued to exhibit the remnants of the slow (0-30 m a^{-1}) splaying flow pattern recorded in 1990-1991 (Figure 6).

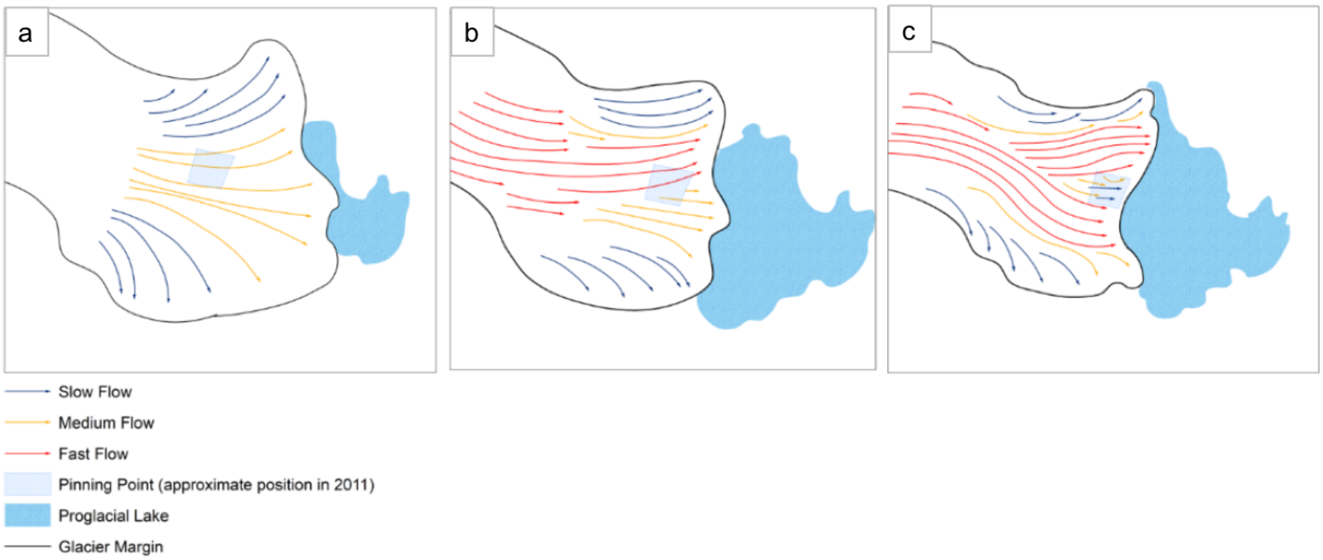

Fig. 6. A three stage conceptual model of glacier evolution at Fjallsjökull, based upon changes in glacier dynamics and structural architecture. Stage 1 (a) represents relatively slow flow velocities, arranged in a splaying pattern. Stage 2 (b) represents an increase in flow velocities and the development of a fast flow 'corridor' in the north. Stage 3 (c) represents the propagation of a secondary flow 'corridor' in the south of the terminus.

Structural Architecture of Fjallsjökull

Between 1982 and 2011 the structural evolution of Fjallsjökull was dominated by a transition from a radial fracture pattern towards a fracture pattern characterised by a series of dextral strike-slip faults. Furthermore, our results show structural evolution towards the calving front. These results support the surface velocity dataset, and further evidence the development of an increasingly concentrated flow regime, through which a pulse of relatively faster flowing ice migrated towards the terminus.

In 1982, the marginal zone of Fjallsjökull could be divided into 45 domains and two key structural zones: the Northern Marginal Zone and the Structurally Complex Frontal Zone (Figure 7). The Northern Marginal Zone included Domains 5 and 11, which were characterised by arcuate, open (∼ 3-5 m wide) fractures (crevasses) that formed a distinct splaying/ radial pattern (Figure 7). This splaying pattern was orientated W-E towards the centre line of the glacier, and NNW-SSE at its margin, as the orientation of the fractures reflected the lateral spreading of the ice within the piedmont zone of the glacier's terminus. The Structurally Complex Frontal Zone in 1982 was comprised of 41 individual domains, reflecting the structural complexity of this part of Fjallsjökull (Figure 7). The majority of fractures within this area were weakly curved to straight, open features which were aligned parallel to the flow direction (WNW-

ESE) of the glacier (e.g. Domains 12, 15, 16, and 18). In addition, a series of transverse to flow, arcuate fractures were also identified up to 300 m up-glacier of the calving front (Figure 7). These fractures were predominantly open (∼ 3-5 m wide), straight, steeply dipping, and closely spaced (e.g. Domains 8, and 29) (Figure 7). Arcuate, up-ice dipping banding was also identified in 1982. The banding was comprised of alternating dark and light layers (typical of Ogive banding), which was made of short (50 to 100 m long), and thin (1 to 10 m wide) segments. The banding was weakly crenulated, with fold wavelengths between 5 and 50 m, and amplitudes between 1 and 10 m.

As in 1982, two key structural zones, the Northern Marginal Zone and the Structurally Complex Frontal Zone, were identified in the lower reaches of Fjallsjökull on the 1994 image (Figure 8). The Northern Marginal Zone changed little since 1982, and its structure was characterised by a series of arcuate, closely spaced, open (∼ 2-9 m wide) fractures (crevasses), arranged in a radial/ splaying pattern (e.g. Domain 11) (Figure 8). The spread in orientations for this zone was greater than in 1982, and fractures were orientated in a SW-NE to WSE-ENE direction (Figure 8).

In the Structurally Complex Frontal Zone in 1994, the surface fracturing was more complex than in 1982 (Figure 8). This structurally complex zone was dissected by several sets of steeply dipping, straight, open (∼ 1.5 to 10 m wide) fractures, which occurred approximately parallel to the calving front (e.g. Domain 12) (Figure 8). These fractures cross-cut and offset a number of flow-parallel fracture sets, which are inferred to have formed in response to an earlier phase of deformation within the ice (Figure 8). In addition, like in 1982, arcuate fracture patterns were also identified. One arcuate fracture pattern was positioned 500 m up-glacier of a prominent headland, and was comprised of a series of concave, down-ice dipping, open fractures belonging to four key Domains (Domains 9, 19, 20 and 29), which were arranged to form a distinct semi-circular geometry (Figure 8). Similarly, a sweeping, arcuate fracture pattern, positioned 160 m up-glacier of a prominent embayment and formed by Domains 8 and 44 was also identified (Figure 8). Fractures within both domains were straight to weakly curved, those belonging to Domain 8 trended in a SW-NE direction, whilst those belonging to Domain 44 trended in a NW-SE direction (Figure 8).

Asymmetrical, weakly crenulated Ogive banding, with wavelengths of 20 to 50 m and amplitudes of 10 to 20 m was also identified in 1994. This banding was predominantly identified towards the glacier's Northern Marginal Zone. However, within the Structurally Complex Frontal Zone this banding became largely overprinted or obscured as a result of locally intense brittle fracturing, although some small discrete patches of banding were still identified (Figure 8).

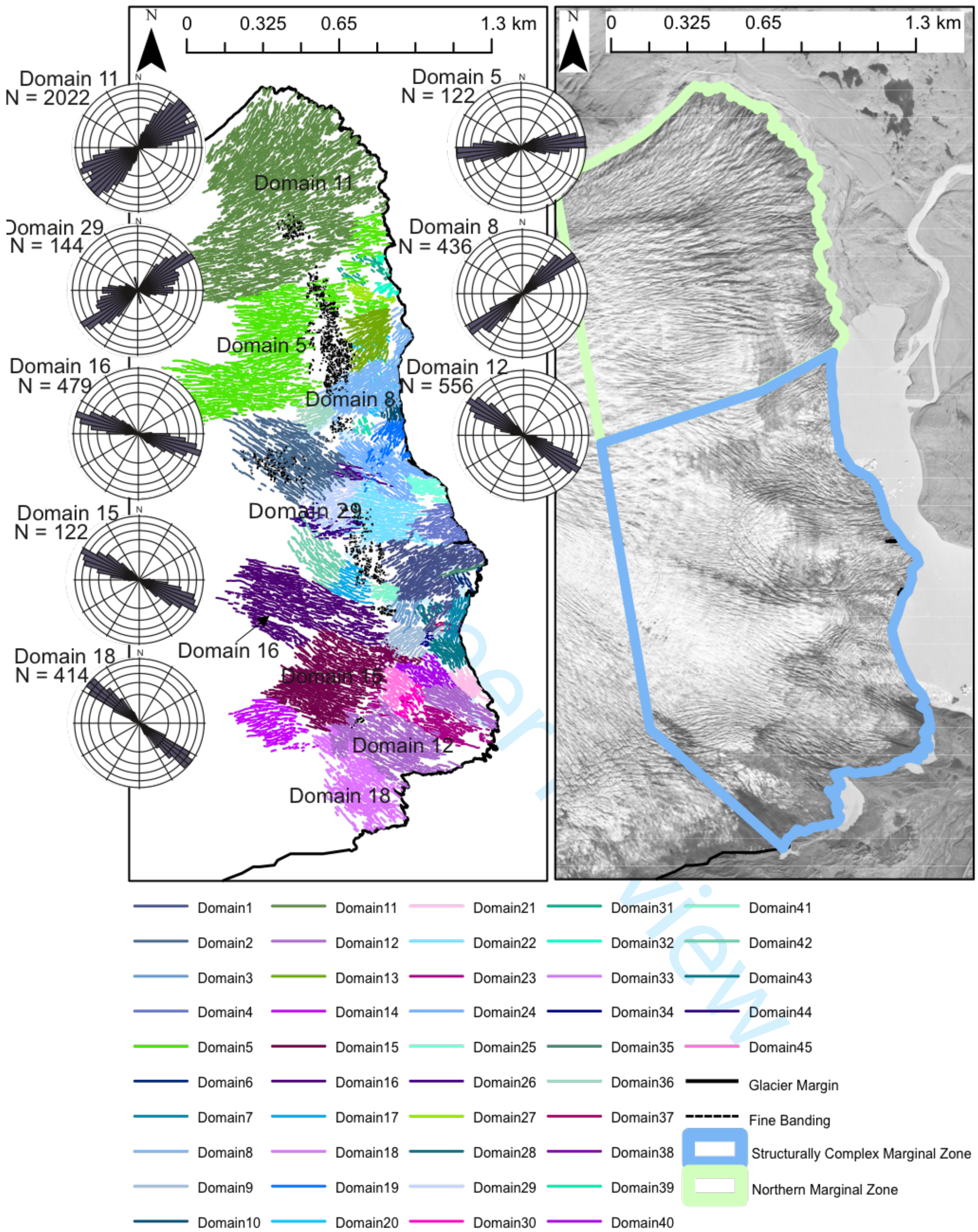

Fig. 7. a) Mapped surface structures at Fjallsjökull's terminus in 1982, key domains are labeled and are also represented by rose diagrams, b) The corresponding aerial photo, from which the surface structures were mapped (acquisition date: 20th August 1982, obtained from: The National Land Survey of Iceland (http://www.lmi.is/wp-content/uploads/2013/10/License-for-use-of-free-NLSI-data-General-Terms.pdf)).

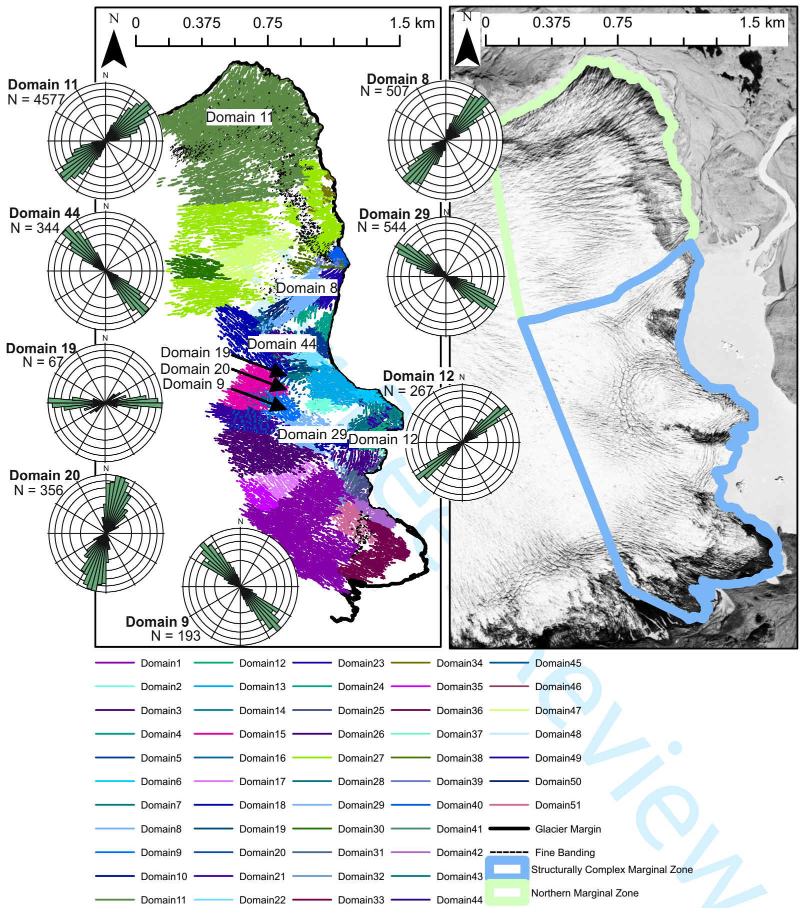

Fig. 8. a) Mapped surface structures at Fjallsjökull's terminus in 1994, key domains are labeled and are also represented by rose diagrams, b) The corresponding aerial photo, from which the surface structures were mapped (acquisition date: 9th August 1994, obtained from: The National Land Survey of Iceland (http://www.lmi.is/wp-content/uploads/2013/10/License-for-use-of-free-NLSI-data-General-Terms.pdf)).

Detailed mapping of the 2011 imagery has enabled the lower reaches of Fjallsjökull to be divided into five key zones; (i) a Structurally Complex Frontal Zone, (ii) a Southern Marginal Zone, (iii) a Southern Central Zone, (iv) a Northern Central Zone and (v) the Northern Marginal Zone (Figure 9).

The Northern Marginal Zone consisted of a single domain (Domain 11), this domain was charaterised by a marked arcuate pattern of hook-shaped fractures, which curved towards the glacier margin, and trended from a SW-NE direction approximately 1.9 km up-glacier to a WSW-ENE direction closer to the glacier's terminus (Figure 9). Overall, the Northern Marginal Zone changed little between 1982 and 2011 (Figure 9). The Southern Marginal Zone identified in 2011 was also characterised by an arcuate pattern of approximately N-S trending, sub-vertical fractures (predominantly belonging to Domain 16), that curved towards the glacier margin (Figure 9).

The Southern Central Zone was positioned between the Southern Marginal Zone and Northern Central Zone (Figure 9). It was comprised of two main domains (Domains 12 and 15), which formed a sigmoidal to s-shaped pattern (Figure 9). This geometry was consistent with fractures which formed as en-echelon tension fissures in response to brittle-ductile shearing of the ice (Figure 9). These fracture sets defined a set of three prominent Y-type dextral strike-slip shear zones (Figure 9). All three shear zones could be traced laterally for up to 2.5 km, and were in the order of 0.6 km wide (Figure 9). The cross-cutting relationship between the individual domains within each shear zone enabled a relative chronology of shear zone formation to be established (Figure 9). The relatively wide shear zone 1 formed first and was later cross cut by the much narrower shear zone 2 (Figure 9). Both shear zones 1 and 2 were cross cut by the relatively younger shear zone 3, with the progressive narrowing of the shear zones possibly reflecting the greater partitioning of the brittle-ductile shear within the ice as deformation continued (Figure 9). Furthermore, these cross-cutting relationships and narrowing of the shear zones suggests that over time there was a transition towards an increasingly concentrated flow regime along the glacier's central axis.

The Northern Central Zone was located immediately to the north of the Southern Central Zone and was characterised by a series of sweeping, arcuate fractures trending in a WSW-ENE direction with increasing proximity to the glacier's terminus (Figure 9). The fractures within this zone were predominantly open (6 m wide), arcuate, and closely spaced (e.g. Domains 8 and 13) (Figure 9). Between the glacier terminus and 1.4 km up-glacier, the boundary defining the Northern and Southern Central Zones was defined by a set of well-developed longitudinal fractures and strike-slip faults (Figure 9). Further up-glacier, a set of open (2-7 m wide), semi-arcuate and sub-vertical fractures belonging to Domains 2 and 15 overprinted the fractures forming this boundary (Figure 9). Both Domains were characterised by a series of sigmoidal to s-shaped fractures, defining a series of small shear zones, consistent with brittle-ductile shearing within the ice (Figure 9). Domain 15 was situated up-glacier of Domain 2, and appears to have truncated the fractures identified within Domain 2 (Figure 9).

The Structurally Complex Frontal Zone was characterised by cross-cutting relationships between the individual structural domains, accompanied by marked variation in fracture orientations. Adjacent domains were often composed of fracture sets orientated perpendicular to one another (Figure 9). Overall, fractures within the Structurally Complex Frontal Zone were typically straight, steeply dipping, and open.

In addition to the structures described above, Ogive banding was also prominent across Fjallsjökull in 2011. Each band was 1 to 10 m in width and composed of numerous short (50 to 100 m long) segments (Figure 9). The Ogive banding was characterised by marked spatial variations across the width of the terminus. The southern and northern marginal zones were characterised by simple, curved banding. Contrastingly, within the southern and northern central zones, the Ogive bands were dissected and modified by a combination of both brittle and ductile shear boundaries, which were associated with changes in the glacier's flow regime, as the centre of the glacier transferred a pulse of fast flowing ice towards the frontal margin (Figure 9).

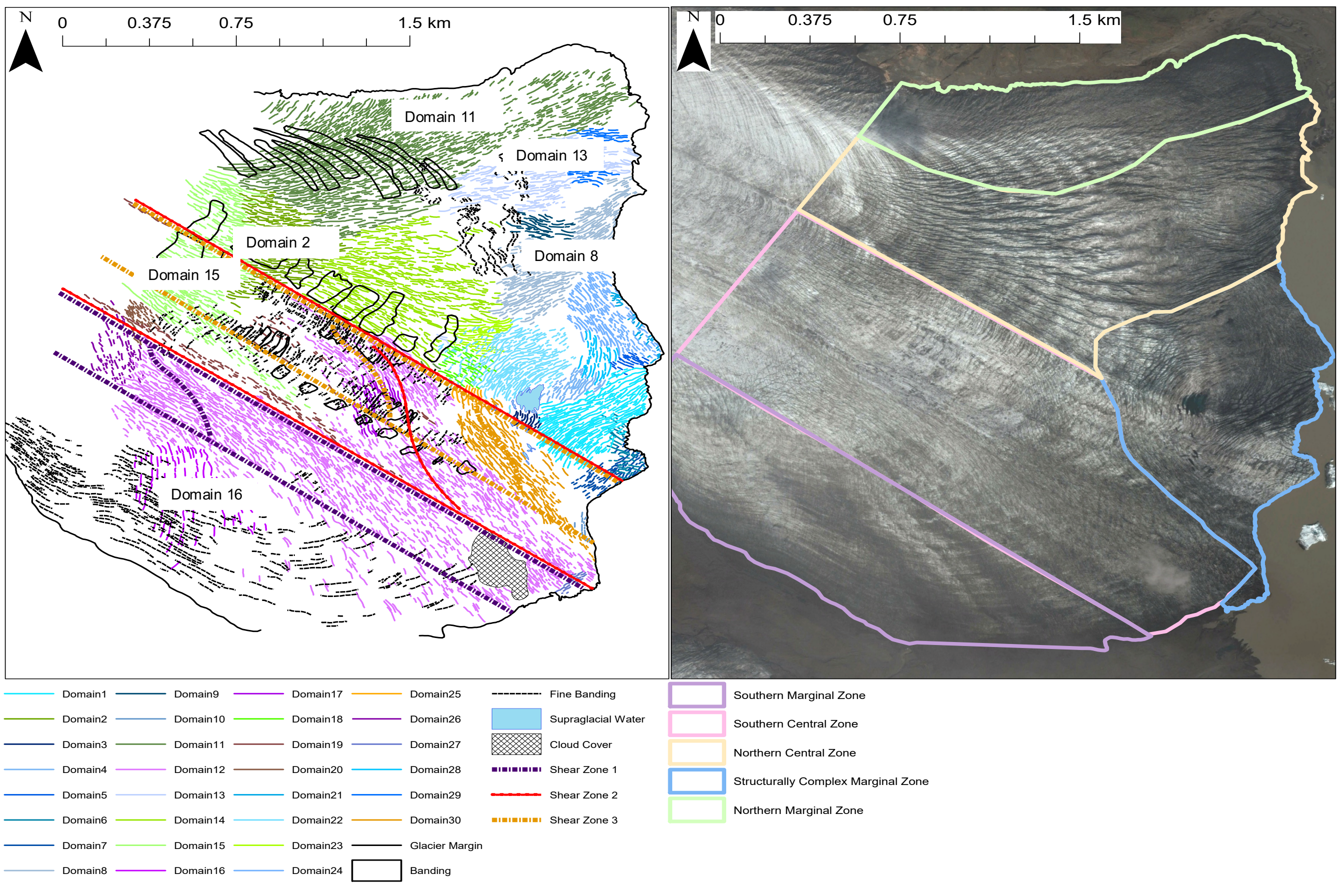

Fig. 9. a) Mapped surface structures at Fjallsjökull's terminus in 2011, key domains are labelled and are also represented by rose diagrams, b) The corresponding satellite image for the 29th June 2011, from which the surface structures were mapped (a Digital Globe Quick Bird image, downloaded via Google Earth).

DISCUSSION

Terminus Position

Fjallsjökull's lake-terminating margin retreated by 1.21 km between 1973 and 2016 (Figure 2) with the rate of retreat increasing significantly in 2001, 2009, and 2011 (Table 1). These findings are corroborated by earlier field observations in Hannesdóttir and others (2015) who measured the retreat of the margin between 1970 and 2010 at a single point on the land termination section of the glacier. The greater retreat rates obtained during the present study (870 m of retreat in the period 1973 to 2010) compared to the study by Hannesdóttir and others (2015) (500 m of retreat between 1973 and 2010), can be partially explained by the differences between the methodologies used, but also by the fact that the lake-terminating portion of the margin is likely to retreat at a much faster rate than its land-terminating margin as a result of mass loss by calving in addition to surface ablation (Benn and others, 2007; Carrivick and Tweed, 2013).

The temporal pattern of terminus retreat at Fjallsjökull is also comparable to retreat patterns observed on many of Vatnajökull's outlet glaciers (e.g. Skalafellsjökull and Fláajökull) between ∼1970 and 2010 (Schomacker, 2010; Hannesdóttir and others, 2015). In particular, the majority of Vatnajökull's outlet glaciers exhibited marked increases in their rate of retreat from ∼1998 onwards (Hannesdóttir and others, 2015). For example, between 1998 and 2010 and following a period of slow retreat, Skalafellsjökull and Fláajökull retreated by 350 m and 538 m respectively (Hannesdóttir and others, 2015). The switch to increased retreat rates at Fjallsjökull, therefore, appears to be part of a wider regional trend.

Lake Area Change

Fjallsárlón increased by 2.72 km^2 between 1973 and 2016, which was coincident with the continued development and expansion of other Icelandic proglacial lakes, particularly for outlet glaciers belonging to Vatnajökull (e.g. Breiðamerkurjökull, Svínafellsjökull, and Skaftafellsjökull) (Schomacker, 2010). Furthermore, statistically significant increases in lake growth in 2001, 2009, and 2011 coincided with the statistically significant increases in terminus retreat rates for Fjallsjökull. A close correspondence between lake growth, accelerated retreat, and increased flow velocities has also been observed at Breiðamerkurjökull (Storrar and others, 2017). Furthermore, at the same location, marked ice surface lowering and terminus retreat was observed (Storrar and others, 2017). Therefore, it appears that water depth exerts a key control on calving activity, surface lowering, and acceleration of Breiðamerkurjökull (Storrar and others, 2017).

Comparably, flow velocities at Fjallsjökull increased between 1999-2000 and 2014-2015, with the greatest velocities corresponding to the deepest parts of the subglacial trench, where the lake depth will be greatest.

Proglacial lake growth can initiate retreat through a number of processes. For example, it can lead to enhanced melt at the water line, enhanced melt below the waterline, and increased torque in response to an increase in buoyant forces (Benn and others, 2007; Dykes and others, 2011). These processes promote calving activity, and facilitate terminus retreat. Therefore, it is suggested that the observed co-incident increases in terminus retreat and lake expansion at Fjallsjökull are likely driven by processes such as torque and thermo-erosion as its proglacial lake expands. The portion of Fjallsjökull's terminus that was lake terminating increased by 40 % over the study period. This may have led to increased, vulnerability of the terminus to calving events and, therefore, increased the rate of retreat.

Air Temperatures: Implications for Thinning, Terminus Retreat, and Lake Expansion

Our findings suggest that air temperatures may strongly influence the rates of surface elevation change, terminus retreat, and lake expansion at Fjallsjökull (Figures 2, 3, and 4). Over the study period, mean annual air temperatures, mean summer surface air temperatures, and PDD all rose by 2.1°C, 1.5 °C, and 511.3 respectively (Figure 4). Furthermore, change-point analysis revealed statistically significant breaks in mean annual surface air temperatures in 1979 and 1992, in PDD in 1984 and 2001, and in mean summer surface air temperatures in 2015 (Table 2). In addition, statistically significant breaks in 2001 (PDD) and 2015 (mean summer surface air temperatures) coincided with/ briefly preceded statistically significant accelerations in the retreat rate and rate of lake area increase at Fjallsjökull, which occurred in 2001, 2009, and 2011 (Table 1). No clear relationship between precipitation and retreat rates was observed. However, this may be due to unreliable precipitation readings, resulting predominantly from wind induced undercatch (e.g. Yang and others, 1999).

We suggest that the observed shifts to significantly warmer air temperatures in 1979 and 1992, and to significantly warmer summer air temperatures in 2015 may have led to increased thinning and ablation at Fjallsjökull. Available data show thinning rates averaging -4.9 m a^{-1} and reaching up to -43.6 m a^{-1} for 2012 to 2013 (Figure 3). This thinning is likely to have contributed substantially to the expansion of Fjallsárlón as meltwater was ponded in the evolving proglacial lake basin. In addition, thinning can result in increased calving activity by (i) increasing the vulnerability of the ice to fractures, (ii) causing an increase in velocities, which results in longitudinal stretching and increased crevassing, and (iii) bringing the terminus nearer to flotation, which increases the potential for full thickness fracturing (Benn and others, 2007). Furthermore, when a terminus transitions from grounded to floating conditions, it experiences a reduction in resistive stresses, and is therefore more susceptible to increased velocities and retreat rates (Joughin and others, 2008).

Similarly to Fjallsjökull, dynamic responses to rising air temperatures and resultant glacier thinning have been previously observed across numerous glaciers elsewhere globally. For example, in Greenland, thinning of inland ice at Helmheim led to a reduction in resistive forces and increased buoyancy of the terminus, which subsequently resulted in increased flow velocities and calving activity (Howat and others, 2005). Furthermore, at Tasman Glacier, a lake calving glacier in New Zealand, downwasting and thinning of the ablation zone has been observed throughout the 20th Century, in line with climate warming. Between 1890 and 1986, some areas of the glacier thinned by 115 m to 185 m (Dykes and others, 2011). Terminus retreat at Tasman Glacier then began in late 20th century; between 2000 and 2006, the average retreat rate was 54 m a^{-1} (Dykes and others, 2011). We suggest that similar processes and feedbacks are operating at Fjallsjökull, in line with rising atmospheric temperatures and resultant thinning.

Increased glacial retreat in response to atmospheric warming has also been seen at many other Icelandic outlet glaciers, including Sólheimajökull, Hyrningsjökull, Morsárjökull, Skaftafellsjökull (Sigurdsson and others, 2007), and Kvíárjökull (Bennett and Evans, 2012). At Kvíárjökull, the area of the glacier snout decreased by more than 5 % a^{-1} between 1998 and 2003, which coincided with a 0.45 °C increase in average summer temperatures (Bennett and Evans, 2012). Furthermore, at Kvíárjökull, no correlation between precipitation and the rate of ice loss is found (Bennett and Evans, 2012). These observations, therefore, identify the significance of rising air temperatures for mass loss from Icelandic outlet glaciers. However, no studies have considered in detail the relationship between proglacial lake growth at Icelandic outlet glaciers and trends in air temperatures. Although, in the Himalaya (e.g. King and others, 2016; Gardelle and others, 2011), and the Central Tibetan Plateau (Wang and others, 2013), co-incident increases in proglacial lake size and air temperatures have been recorded. For example, in the Tibetan Plateau's Western Nyainqentanglha region, direct links between climate warming, glacier ablation and proglacial lake expansion have been made, with the region's glacier's reducing by 22 % in aerial extent between 1977 and 2010, and the area of glacier lakes increasing by 173 % between 1972 and 2009 (Wang and others, 2013). We identify similar patterns at Fjallsarlön, as the lake extent increased by 303 % in response to increasing air temperatures between 1973 and 2016.

Concentrated flow at Fjallsjökull – a conceptual model

The proposed model combines the observed changes in surface velocities and surface structures to explain the development of a pulse of relatively 'faster flow' through distinct corridors, which conveyed ice to the calving front (Figure 6). Three key stages have been identified: (1) Prior to 2000, a period of relatively slow flow (Figures 5a and 5b) under a splaying flow regime. This is typical of ice spreading laterally to form a piedmont lobe as it leaves the confines of its valley (Figure 6a); (2) a period between 2001 and 2014 in which there was the development of a pulse of relatively faster flow and the development of the northern 'corridor' (Figures 5d, e and 6b); and (3) the development of a secondary, southern fast flow 'corridor' (Figures 5f and 6c).

Stage 1 (1990-2000)

This stage lasted from 1990 to 2000 (Figures 5a, 5b and 6a) and resulted in a radiating fan-like internal structural architecture to the glacier (Figure 8) with relatively faster flow ($\sim$ 60- 100 m a^{-1}) along the centre line of the glacier and relatively slower flow at its margins ($\sim$20 m a^{-1}) due to frictional drag along the valley walls. The structural architecture of the glacier shown on the 1994 structural map (Figure 8) was consistent with the ice undergoing longitudinal compression and lateral extension as it flowed out of its confining valley (c.f. Colgan and others, 2016 and references therein). The observed structural regime at Fjallsjökull is expected for glaciers that terminate in a piedmont lobe (Post, 1972), as the margins are exposed to large transverse shear stresses, resulting in relatively slow flow at the glacier's margins (Lawson and others, 1994). Similar splaying structures have previously been reported in Iceland (Phillips and others, 2017), New Zealand (Appleby and others, 2010), and Alaska (Sharp and others, 1988).

Stage 2 (2000-2015)

Stage two was characterised by increased surface velocities. Locally, the surface velocities at Fjallsjökull increased by approximately 30 m a^{-1} between 2000-2001 and 2001-2002 (Figure 5), coinciding with a statistically significant change point in terminus retreat rates and lake expansion in 2001, in addition to an increase in the structural complexity of the glacier (Table 1). Furthermore, the increase in surface velocities followed identified change-points in atmospheric air temperatures (1979 and 1992) and in PDD (1984 and 2001) (Table 2). It can, therefore, be argued that this near-simultaneous acceleration in surface velocities, increase in terminus retreat rates, and increase in lake expansion rates was predominantly driven by rising air temperatures and resultant thinning via surface ablation. Rising air temperatures likely led to persistent and widespread thinning of the terminus, which drove retreat of the glacier terminus, as the glacier became increasingly susceptible to full thickness fracturing (as discussed in section 4.3) (Benn and others, 2007). As the glacier terminus retreated into deeper water, a positive feedback loop likely resulted, further driving increased retreat rates and accelerated ice surface velocities (Benn and others, 2007).

In 2014-2015, a single, northern, 'fast flow' corridor extended from $\sim$ 4 km up-glacier, towards the calving front (see region iv in Figure 5e). This northern corridor of relatively faster flow corresponded to an increase in the structural complexity of the glacier and the forward movement of ice within the corridor, which resulted in shearing at its margins. These shear margins were marked by dextral strike-slip faults (as identified in the 2011 structural map), where Domain 15 locally overprinted Domain 2, approximately 1.4 km up-glacier of the calving front (Figure 9). The ice within this corridor was also heavily crenulated, with banding exhibiting amplitudes of between 5 and 30 m, indicating marked lateral compression of the ice within this region. Furthermore, the surface velocity results identified the source of this relatively faster flowing pulse of ice to have originated from region (i), not from the accumulation zone on Öræfajökull. The destabilisation of ice in zone (i) may have occurred above the up ice boundary of the bedrock overdeepening, as ice draw down was initiated in response to increased calving activity as the proglacial lake expanded (Figure 10).

Overall, an increase in the calving rate of a glacier, such as Fjallsjökull, may result in the development of a positive feedback loop, as an increase in calving increases the net drawdown of ice through the glacier's system, steepening the glacier's surface, and further facilitating an increase in mass loss as the glacier retreats into deeper water (Carrivick and Tweed, 2013). A similar scenario has been previously observed at Mendenhall Glacier, south-east Alaska; the glacier thinned and retreated into deeper water until it reached flotation and destabilised (Motyka and others, 2003). Once destabilised, the glacier terminus began to calve at an increased rate into its proglacial lake, which facilitated further retreat into deeper water and initiated a positive feedback loop (Motyka and others, 2003).

Stage 3 (2016-2017)

By 2016-2017, an additional, southern 'fast flow' corridor had developed at Fjallsjökull (see region v in Figure 5f). In addition, this second 'fast flow' corridor is represented in the structural data by a series of three dextral strike-slip shear zones, as identified in the 2011 structural assessment (Figure 9). The cross-cutting relationship of the fracture sets in this zone reflected the narrowing of the dextral strike-slip shear zones over time (Figure 9). It is, therefore, argued that the progressive narrowing of these shear zones represented the narrowing of the fast flow 'corridor' over time, which culminated in the scenario shown in the 2016-2017 velocity output (Figure 5f).

It is likely that the spatial arrangement of Fjallsjökull's flow regime was primarily influenced by the underlying bedrock topography (Figure 10) (Magnússon and others, 2012). This may have increasingly impacted surface ice velocities as the glacier retreated back into its over-deepening, and as it thinned under rising air temperatures. The two identified 'fast flow' corridors at Fjallsjökull were underlain by prominent depressions in the bedrock, which will be further discussed in section 4.5 (Figure 10) (Magnússon and others, 2012). Where the glacier retreated across these depressions, processes including buoyancy driven calving, torque due to buoyant forces, and thermally induced melt increased where the glacier entered deeper water (Benn and others, 2007; Nick and others, 2009; Porter and others, 2014; Carr and others, 2015). The spatial signature of velocity changes at Fjallsjökull, therefore, suggest that the observed increases in velocities resulted from retreat rather than increased basal lubrication. This argument is supported by the work of Tedstone and others (2015), who suggest that hydrodynamic coupling at the ice bed interface may reduce net ice surface velocities, as increased meltwater input to the ice bed interface results in the development of an increasingly channelised drainage system, which exports water delivered to the ice-bed interface before it can act as a basal lubricant.

Bedrock Topography

Whilst the dynamic changes observed at Fjallsjökull were initiated by rising air temperatures, these changes were likely sustained and/or accelerated by local variations in the underlying bedrock topography. Magnússon and others (2012) provide bedrock topography data for Fjallsjökull, which is predominantly based on points collected through a Radio Echo Sounding survey, conducted between 1998 and 2006. This data has an error of $\pm$ 20 m (Magnússon and others, 2012). Where data was sparse, they calculate pseudo profiles by estimating the relationship between the surface slope and the ice thickness (Magnússon and others, 2012). These data were then interpolated to provide a contour map of Fjallsjökull (Figure 10) (Magnússon and others, 2012). Both Fjallsjökull and Fjallsarlön sit within a $\sim$ 3 x 4 km subglacial trough, which lies up to 206 m below sea-level (Figure 10) (Magnússon and others, 2012). Subglacial troughs exist beneath a number of outlet glaciers flowing from the Vatnajökull Ice-Cap (e.g. Breiðamerkurjökull, Skaftafellsjökull, Svínafellsjökull), and often dam pro-glacial lakes as glaciers retreat (Schomacker, 2010) (Figure 1). As Fjallsjökull retreated across the bedrock depression, its proglacial lake was able to expand and likely deepen, facilitating further acceleration, thinning, and retreat of the glacier into deeper water (Meier and Post 1987; Vieli and others, 2002; Benn and others, 2007; Joughin and others, 2008; Carr and others, 2013; Hill and others, 2018).

It is, therefore, likely that the initiation of relatively faster flowing surface velocities at Fjallsjökull was in response to the expansion of Fjallsárlón, which resulted in increased calving activity and, as a result, increased ice draw down. We propose that the identified pulse of relatively fast flowing ice identified from the early 2000's onwards was initiated at region (i), 4 km up glacier of the terminus (Figure 10). This region sits immediately down-ice of where the bedrock overdeepening begins, and is likely to have been the initial source of ice destabilisation in response to increased calving activity and ice draw down.

Secondly, two deeply incised channels exist within Fjallsjökull's bedrock topography, which currently underlie portions of the northern and southern portions of Fjallsjökull's terminus, and likely to be controlling the location of the increasingly channelised flow (Figure 10). The northern channel is elongate, and extends from $\sim$ 6.7 km up glacier of the terminus position in 2011 towards the calving front, and reaches a maximum depth of 200 m below sea-level (see ii in Figure 10). The southern channel is $\sim$ 2 km by 2 km, and extends towards the calving front, reaching a maximum depth of 120 m below sea-level (see iii in Figure 10). These small-scale topographic variations likely influence local glacier dynamics, and in particular, the rate of retreat and glacier surface velocities. Where the glacier overlies localised deep channels, the rate of buoyancy driven calving may be greater, as processes such as torque due to buoyant forces and thermally induced melt are greater at depth (Todd and Christoffersen, 2014). Furthermore, these two channels coincide with the two identified 'fast flow corridors', which develop at Fjallsjökull between 2014 and 2017 (Figure 5). It is, therefore, likely that where the glacier overlies these relatively deep channels and experiences an increase in buoyancy driven calving, a positive feedback loop is initiated, facilitating further acceleration, draw down of up-glacier ice, thinning, and further retreat (Meier and Post 1987; Vieli and others, 2002; Benn and others, 2007; Joughin and others, 2008; Carr and others, 2013; Hill and others, 2018).

At Breiðamerkurjökull, the large outlet glacier neighboring Fjallsjökull, alterations in the glacier's dynamic regime have also been attributed to small scale variations in the underlying topography (Storrar and others, 2017). Part of Breiðamerkurjökull terminates in a large proglacial lake, Jökulsárlón, and sits

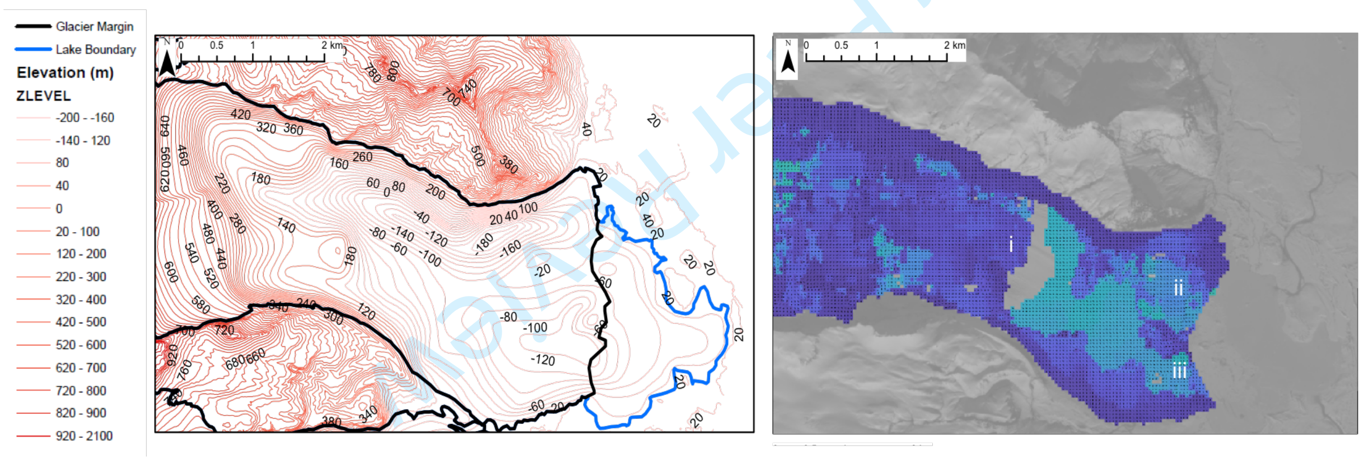

Fig. 10. (a) Bedrock topography dataset for Fjallsjökull displayed as a contour map with intervals of 20 m. (b) Calculated surface velocity data for Fjallsjökull in 2016-2017, based on two Sentinel-2 MSI images. Labels i-ii indicate notable features that reveal links between the surface velocities and bed topography data. i indicates the position of the northern fast flow 'corridor', and ii indicates the southern fast flow corridor, both 'corridors' align with a depression in the bedrock.

in an over-deepening that is up to 300 m below sea level (Storrar and others, 2017). Retreat rates and thinning rates are greatest here, where the glacier sits above a pronounced over-deepening (Nick and others, 2009; Storrar and others, 2017). Evidence indicates that, like Fjallsjökull, the retreat of Breiðamerkurjökull over the Jökulsárlón trench drove a positive feedback loop, which led to increased rates of ice flow and ice surface draw down. This relationship was, again, predominantly attributed to the glacier's retreat into deeper water, which facilitated increased calving activity (Nick and others, 2009; Storrar and others, 2017). We, therefore, infer that similar processes are operating at Fjallsjökull, and that retreat over the overdeepening encourages increased surface velocities and ice mass loss.

CONCLUSIONS

Overall, this study highlights the significance of glacier specific (e.g. bedrock topography) and non-glacier specific (e.g. climate) controls on the dynamic and structural regime of Fjallsjökull. The combination of the structural and velocity data has provided a greater insight into the spatial complexities of the glacier's evolution. We identified statistically significant change-points for both terminus position and lake area change in 2001, 2009, and 2011. The synchronous increased rates of terminus retreat and lake expansion reveals a link between the two processes, which we propose is driven by an increase in longitudinal stresses acting on the glacier terminus as the proglacial lake extent increases. We identify rising atmospheric air temperatures as a key control on terminus position and lake area at Fjallsjökull. Our conceptual model, which combines an assessment of changes to the glacier's surface velocities and structural architecture over the study period, reveals the development of an increasingly spatially complex flow regime over time, characterised by a series of 'fast flow' corridors. Dextral-strike slip faults facilitate this flow regime, as they allow corridors of faster flowing ice to propagate towards the terminus. Furthermore, we argue that the spatial complexities of the concentrated flow regime are governed by the bedrock topography that underlays the glacier. The influence of this bedrock topography on the glacier's dynamic and structural regime appears to have increased throughout the study period, as the glacier has thinned due to rising ATT.

REFERENCES

AMAP (2017). Arctic Monitoring and Assessment Programme (AMAP)-Progress Report.

Appleby JR, Brook MS, Vale SS and Macdonald-Creevey AM (2010) Structural glaciology of a temperate maritime glacier: Lower fox glacier, New Zealand. Geogr. Ann. Ser. A Phys. Geogr. 92(4), 451–467 (doi:10.1111/j.1468-0459.2010.00407.x)

Barr, I., Dokukin, M., Kougkoulos, I., Livingstone, S., Lovell, H., Małecki, J., and Muraviev, A., 2018. Using ArcticDEM to Analyse the Dimensions and Dynamics of Debris-Covered Glaciers in Kamchatka, Russia. Geosciences, 8 (6), 216.

Benn DI, Warren CR and Mottram RH (2007) Calving processes and the dynamics of calving glaciers. Earth-Science Rev. 82(3–4), 143–179 (doi:10.1016/j.earscirev.2007.02.002)

Bennett GL and Evans DJA (2012) Glacier retreat and landform production on an overdeepened glacier foreland: The debris-charged glacial landsystem at Kvíárjökull, Iceland. Earth Surf. Process. Landforms 37(15), 1584–1602 (doi:10.1002/esp.3259)

Björnsson H, Pálsson F, Gudmundsson S, Magnússon E, Adalgeirsdóttir G, Jóhannesson T, Berthier E, Sigurdsson O and Thorsteinsson T (2013) Contribution of Icelandic ice caps to sea level rise: Trends and variability since the Little Ice Age. Geophys. Res.Lett. 40(8), 1546–1550 (doi:10.1002/grl.50278)

Björnsson H and Pálsson F. (2008). Icelandic glaciers. Jökull, 58(58), 365-386.

Bolch T, Pieczonka T and Benn DI (2011) Multi-decadal mass loss of glaciers in the Everest area (Nepal Himalaya) derived from stereo imagery. Cryosphere 5(2), 349–358 (doi:10.5194/tc-5-349-2011)

Carr JR, Stokes CR and Vieli A (2017) Threefold increase in marine-terminating outlet glacier retreat rates across the Atlantic Arctic: 1992–2010. Annals of Glaciology. 72–91 (doi:10.1017/aog.2017.3)

Carr JR, Vieli A, Stokes CR, Jamieson SSR, Palmer SJ, Christoffersen P, Dowdeswell JA, Nick FM, Blankenship DD and Young DA (2015) Basal topographic controls on rapid retreat of Humboldt Glacier, northern Greenland. J. Glaciol. 61(225), 137–150 (doi:10.3189/2015JoG14J128)

Carr JR, Stokes C and Vieli A (2014) Recent retreat of major outlet glaciers on Novaya Zemlya, Russian Arctic, influenced by fjord geometry and sea-ice conditions. J. Glaciol. 60(219), 155–170 (doi:10.3189/2014JoG13J122)

Carr JR, Vieli A and Stokes C (2013) Influence of sea ice decline, atmospheric warming, and glacier width on marine-terminating outlet glacier behavior in northwest Greenland at seasonal to interannual timescales. J. Geophys. Res. Earth Surf. 118(3), 1210–1226 (doi:10.1002/jgrf.20088)

Carrivick JL and Tweed FS (2013) Proglacial Lakes: Character, behaviour and geological importance. Quat. Sci. Rev. 78, 34–52 (doi:10.1016/j.quascirev.2013.07.028)

Colgan W, Rajaram H, Abdalati W, McCutchan C, Mottram R, Moussavi MS and Grigsby S (2016) Glacier crevasses: Observations, models, and mass balance implications. Reviews of Geophysics 54(1), 119–161 (doi:10.1002/2015RG000504)

Dykes RC, Brook MS, Robertson CM and Fuller IC (2011) Twenty-First Century Calving Retreat of Tasman Glacier, Southern Alps, New Zealand. Arctic, Antarct. Alp. Res. 43(1), 1–10 (doi:10.1657/1938-4246-43.1.1)

Eckley IA, Fearnhead P and Killick R (2011) Analysis of changepoint models. Bayesian Time Series Models. 205–224 (doi:10.1017/CBO9780511984679.011)

Evans D and Twigg D (2002) The active temperate glacial landsystem: a model based on Breiðamerkurjökull and Fjallsjökull, Iceland. Quat. Sci. Rev. 21(20), 2143–2177 http://www.sciencedirect.com/science/article/pii/S02

Fahnestock M, Scambos T, Moon T, Gardner A, Haran T and Klinger M (2015) Rapid large-area mapping of ice flow using Landsat 8. Remote Sens. Environ. 185, 84–94 (doi:10.1016/j.rse.2015.11.023)

Flowers, G.E., Marshall, S.J., Björnsson, H., and Clarke, G.K.C., 2005. Sensitivity of Vatnajökull ice cap hydrology and dynamics to climate warming over the next 2 centuries. Journal of Geophysical Research: Earth Surface, 110 (2), F02011.

Foresta L, Gourmelen N, Pálsson F, Nienow P, Björnsson H and Shepherd A (2016) Surface elevation change and mass balance of Icelandic ice caps derived from swath mode CryoSat-2 altimetry. Geophys. Res. Lett. 43(23), 12,138-12,145 (doi:10.1002/2016GL071485)

Gardelle J, Arnaud Y and Berthier E (2011) Contrasted evolution of glacial lakes along the Hindu Kush Himalaya mountain range between 1990 and 2009. Glob. Planet. Change 75(1–2), 47–55 (doi:10.1016/j.gloplacha.2010.10.0

Hannesdóttir H, Björnsson H, Pálsson F, Aðalgeirsdóttir G and Guðmundsson S (2015) Changes in the southeast Vatnajökull ice cap, Iceland, between ∼ 1890 and 2010. Cryosph. 9, 565–585 (doi:10.5194/tc-9-565-2015)

Hill EA, Carr JR, Stokes CR and Gudmundsson GH (2018) Dynamic changes in outlet glaciers in northern Greenland from 1948 to 2015. Cryosph. Discuss., 1–39 (doi:10.5194/tc-2018-17)

Howarth PJ and Price RJ (1969) The proglacial lakes of Breiðamerkurjökull and Fláajökull, Iceland. Geogr. J. 135(part 4), 573–581 http://www.jstor.org/stable/1795105

Howat IM, Joughin I, Tulaczyk S and Gogineni S (2005) Rapid retreat and acceleration of Helheim Glacier, east Greenland. Geophys. Res. Lett. 32(22), 1–4 (doi:10.1029/2005GL024737)

Joughin I, Howat I, Alley RB, Ekstrom G, Fahnestock M, Moon T, Nettles M, Truffer M and Tsai VC (2008) Ice-front variation and tidewater behavior on Helheim and Kangerdlugssuaq Glaciers, Greenland. J. Geophys. Res. Earth Surf. 113(1), F01004 (doi:10.1029/2007JF000837)

Killick, R., Fearnhead, P., and Eckley, I.A., 2012. Optimal detection of changepoints with a linear computational cost. Journal of the American Statistical Association, 107 (500), 1590–1598.

King O, Quincey DJ, Carrivick JL and Rowan A V. (2016) Spatial variability in mass change of glaciers in the Everest region, central Himalaya, between 2000 and 2015. Cryosph. Discuss., 1–35 (doi:10.5194/tc-2016-99)

Larsen SH, Khan SA, Ahlstrøm AP, Hvidberg CS, Willis MJ and Andersen SB (2016) Increased mass loss and asynchronous behavior of marine-terminating outlet glaciers at Upernavik Isstrøm, NW Greenland. J. Geophys. Res. Earth Surf. 121(2), 241–256 (doi:10.1002/2015JF003507)

Lawson WJ, Sharp MJ and Hambrey MJ (1994) The structural geology of a surge-type glacier. J. Struct. Geol. 16(10), 1447–1462 (doi:10.1016/0191-8141(94)90008-6)

Lea JM, Mair DWF and Rea BR (2014) Instruments and Methods: Evaluation of existing and new methods of tracking glacier terminus change. J. Glaciol. 60(220), 323–332 (doi:10.3189/2014JoG13J061)

Lovell A (2016) The drivers of inter-annual outlet glacier terminus change in Victoria Land, Oates Land and George V Land, East Antarctica (1972-2013). http://etheses.dur.ac.uk/11561/

Magnússon E, Pálsson F, Björnsson H and Guðmundsson S (2012) Removing the ice cap of Öraefajokull central volcano, SE-Iceland: Mapping and interpretation of bedrock topography, ice volumes, subglacial troughs and implications for hazards assessments. Jökull, 62, 131-150.

Meier MF and Post A (1987) Fast tidewater glaciers. J. Geophys. Res. 92(B9), 9051–9058 (doi:10.1029/JB092iB09p090

Messerli A and Grinsted A (2015) Image georectification and feature tracking toolbox: ImGRAFT. Geosci. Instrumentation, Methods Data Syst. 4(1), 23–34 (doi:10.5194/gi-4-23-2015)

Moon T and Joughin I (2008) Changes in ice front position on Greenland's outlet glaciers from 1992 to 2007. J. Geophys. Res. Earth Surf. 113(2), F02022 (doi:10.1029/2007JF000927)

Morin P, Porter C, Cloutier M and Howat I (2016) ArcticDEM; A Publically Available, High Resolution Elevation Model of the Arctic. EGU Gen. 18, 8396 http://adsabs.harvard.edu/abs/2016EGUGA..18.8396M

Motyka RJ, O'Neel S, Connor CL and Echelmeyer KA (2003) Twentieth century thinning of Mendenhall Glacier, Alaska, and its relationship to climate, lake calving, and glacier run-off. Glob. Planet. Change 35(1–2), 93–112 (doi:10.1016/S0921-8181(02)00138-8)

Nick FM, Vieli A, Howat IM and Joughin I (2009) Large-scale changes in Greenland outlet glacier dynamics triggered at the terminus. Nat. Geosci. 2(2), 110–114 (doi:10.1038/ngeo394)

Pálsson F, Guðmundsson S, Björnsson H, Berthier E, Magnússon E and Haraldsson HH (2012) Mass and volume changes of Langjokull ice cap, Iceland, similar to 1890 to 2009, deduced from old maps, satellite images and in situ mass balance measurements. Jökull 62, 81–96

Phillips E, Everest J, Evans DJA, Finlayson A, Ewertowski M, Guild A and Jones L (2017) Concentrated, 'pulsed' axial glacier flow: structural glaciological evidence from Kvíárjökull in SE Iceland. Earth Surf. Process. Landforms 42(13), 1901–1922 (doi:10.1002/esp.4145)

Porter DF, Tinto KJ, Boghosian A, Cochran JR, Bell RE, Manizade SS and Sonntag JG (2014) Bathymetric control of tidewater glacier mass loss in northwest Greenland. Earth Planet. Sci. Lett. 401, 40–46 (doi:10.1016/j.epsl.2014.05.058)

Post A (1972) Periodic Surge Origin of Folded Medial Moraines on Bering Piedmont Glacier, Alaska *. J. Glaciol. 11(62), 219–226

Schomacker A (2010) Expansion of ice-marginal lakes at the Vatnaj??kull ice cap, Iceland, from 1999 to 2009. Geomorphology 119(3–4), 232–236 (doi:10.1016/j.geomorph.2010.03.022)

Sharp M, Lawson W and Anderson RS (1988) Tectonic processes in a surge-type glacier. J. Struct. Geol. 10(5), 499–515 (doi:10.1016/0191-8141(88)90037-5)

Sigurdsson O, Jónsson T and Jóhannesson T (2007) Relation between glacier-termini variations and summer temperature in Iceland since 1930. Annals of Glaciology. 170–176 (doi:10.3189/172756407782871611)

Storrar RD, Jones AH and Evans DJA (2017) Small-scale topographically-controlled glacier flow switching in an expanding proglacial lake at Breiðamerkurjökull, SE Iceland. Journal of Glaciology 63(240), 745–750 (doi:10.1017/jog.2017.22)

Tedstone AJ, Nienow PW, Gourmelen N, Dehecq A, Goldberg D and Hanna E (2015) Decadal slowdown of a land-terminating sector of the Greenland Ice Sheet despite warming. Nature 526(7575), 692–695 (doi:10.1038/nature15722)

Todd J and Christoffersen P (2014) Are seasonal calving dynamics forced by buttressing from ice mélange or undercutting by melting? Outcomes from full-Stokes simulations of Store Glacier, West Greenland. Cryosphere 8(6), 2353–2365 (doi:10.5194/tc-8-2353-2014)

Van der Veen CJ (2002) Calving glaciers. Prog. Phys. Geogr. 26(1), 96–122 (doi:10.1191/0309133302pp327ra)

Van Der Veen CJ (1996) Tidewater calving. J. Glaciol. 42(141), 375–385 (doi:10.1179/102453311X13127324303399)

Vieli A, Jania J and Kolondra L (2002) The retreat of a tidewater glacier: Observations and model calculations on Hansbreen, Spitsbergen. J. Glaciol. 48(163), 592–600 (doi:10.3189/172756502781831089)

Vilhjálmsson H (2002) Capelin (Mallotus villosus) in the Iceland–East Greenland–Jan Mayen ecosystem.

academic.oup.com https://academic.oup.com/icesjms/article-abstract/59/5/870/675196

Wang X, Siegert F, Zhou A guo and Franke J (2013) Glacier and glacial lake changes and their relationship in the context of climate change, Central Tibetan Plateau 1972-2010. Glob. Planet. Change 111, 246–257 (doi:10.1016/j.gloplacha.2013.09.011)

Westrin P (2015) External conditions effects on the self-organised criticality of the calving glacier front of Tunabreen, Svalbard. http://www.diva-portal.org/smash/record.jsf?pid=diva2:823789

Yang, D.Q., Elomaa, E., Tuominen, A., Aaltonen, A., Goodison, B., Gunther, T., Golubev, V., Sevruk, B., Madsen, H., and Milkovic, J., 1999. Wind-induced precipitation undercatch of the Hellmann gauges. Nordic Hydrology, 30 (1), 57–80.

731 # APPENDIX

Table A.1. A record of the satellite and aerial images used in the study.

Satellite	Path	Row	ID Number	Satellite Acquisition Date	Method
Landsat8 OLI/TIRS	217	15	LC82170152016271 LGN00	27-Sep-16	Frontal Position and Lake Area Change
Landsat8 OLI/TIRS	217	15	LC82170152015268 LGN00	25-Sep-15	Near-terminus velocity calculations
Landsat8 OLI/TIRS	217	15	LC82170152014233 LGN00	21-Aug-14	Near-terminus velocity calculations
Landsat7 ETM + SLC-off	217	15	LE72170152011265 ASN00	22-Sep-11	Frontal Position and Lake Area Change
Landsat7 ETM + SLC-off	217	15	LE72170152010262 EDC00	19-Sep-10	Frontal Position and Lake Area Change
Landsat7 ETM + SLC-off	217	15	LE72170152002256 EDC00	13-Sep-02	Frontal Position and Lake Area Change
Landsat7 ETM + SLC-off	217	15	LE72170152002128 KIS00	08-May-02	Near-terminus velocity calculations
Landsat7 ETM + SLC-off	217	15	LE72170152001221 KIS00	09-Aug-01	Frontal Position and Lake Area Change

Landsat7 ETM + SLC-off	217	15	LE72170152001109 EDC00	19-Apr-01	Near-terminus velocity calculations
Landsat7 ETM + SLC-off	217	15	LE72170152000107 EDC00	16-Apr-00	Near-terminus velocity calculations
Landsat4-5 TM	216	15	LT52160152009228 KIS00	16-Aug-09	Frontal Position and Lake Area Change
Landsat4-5 TM	217	15	LT52170151998189 KIS00	08-Jul-98	Frontal Position and Lake Area Change
Landsat4-5 TM	217	15	LT52170151994242 KIS00	30-Aug-94	Frontal Position and Lake Area Change, Near-terminus velocity calculations
Landsat4-5 TM	217	15	LT52170151991250 XXX03	07-Sep-91	Frontal Position and Lake Area Change, Near-terminus velocity calculations
Landsat4-5 TM	217	15	LT52170151990247 KIS00	04-Sep-90	Frontal Position and Lake Area Change, Near-terminus velocity calculations

Landsat1-5 MSS	217	15	LM52170151985217 AAA03	05-Aug-85	Frontal Position and Lake Area Change
Landsat1-5 MSS	217	15	LM42170151983188 FFF03	07-Jul-83	Frontal Position and Lake Area Change
Landsat1-5 MSS	217	15	LM12350151973211 FAK03	30-Jul-73	Frontal Position and Lake Area Change
Sentinel-2 MSI	N/A	N/A	L1C_T28WDS_A0088 58_20170303T125255	03-Mar-17	Near-terminus velocity calculations
Sentinel-2 MSI (64.4285218, -15.9372852)	N/A	N/A	S2A_OPER_MSI_L1C _TL_SGS__20160318 T125409_20160318T201 139_A003853_T28WD S_N02 _01_01	18-Mar-16	Near-terminus velocity calculations
Map Data Google Earth Pro, Digital Globe, Image NASA, Image Landsat/ Copernicus V7.1.5.1557.	N/A	N/A	64.023801308°, -16.438297479°.	29-Jun-11	Structural Analysis

Table A.2. The acquisition date of Image A and Image B used for each image pair in the feature tracking analysis, and the temporal gap (in days) between Image A and Image B.

Acquisition Date		Temporal Gap (days)
Image A	**Image B**	
04/09/1990	07/09/1991	368
07/09/1991	30/08/1994	1088
16/04/2000	19/04/2001	368
19/04/2001	08/05/2002	384
21/08/2014	25/09/2015	400

[]

Table A.3. Spatial resolution and image acquisition period of satellite sensors

Satellite	Image Acquisition Period	Spatial Resolution (m)
Landsat 1-5 MSS	1972-2013	60
Landsat 4-5 TM	1988-1991	30
Landsat 7 ETM +	1999-2013	30 (15 for panchromatic)
Landsat 8 OLI/TIRS	2014-ongoing	30 (15 for panchromatic)
Sentinel-2 MSI	2015- ongoing	10
Digital Globe Quick Bird (Google Earth)	2001-2015	2.62

[]

Table A.4. Manual digitisation errors, co-registration errors, and total errors for each satellite sensor used for terminus position and lake area change analysis.

	Error Type	Landsat 1-5	Landsat 4-5	Landsat 7	Landsat 8
Terminus Position	Co-registration (L1-5, 3-5, 7) or Geo-location (L8) (m)	97	30	25	7.8-8.9
	Manual Digitisation (m)	40	4	9	2
	Total (m)	137	34	34	9.8-10.9
Lake Area	Co-registration (L1-5, 3-5, 7) or Geo-location (L8) (m)	97	30	25	7.8-8.9
	Manual Digitisation (m2)	73147	11333	10553	8598
	Manual Digitisation (m)	73	11	11	9
	Total (m)	170	41	36	16.8-17.9

[]

Table A.5. Average RGB values and the respective velocities for stationary points in each image pair. The average surface velocity is indicative of the error associated with each time-step.

	Average RGB Value	Average Surface Velocity (m a-1)
1990-1991	53, 48, 47	8
1991-1994	53, 42, 135	0
2000-2001	53, 48, 147	8
2001-2002	53, 48, 147	8
2014-2015	53, 42, 135	0
2016-2017	53, 46, 142	5

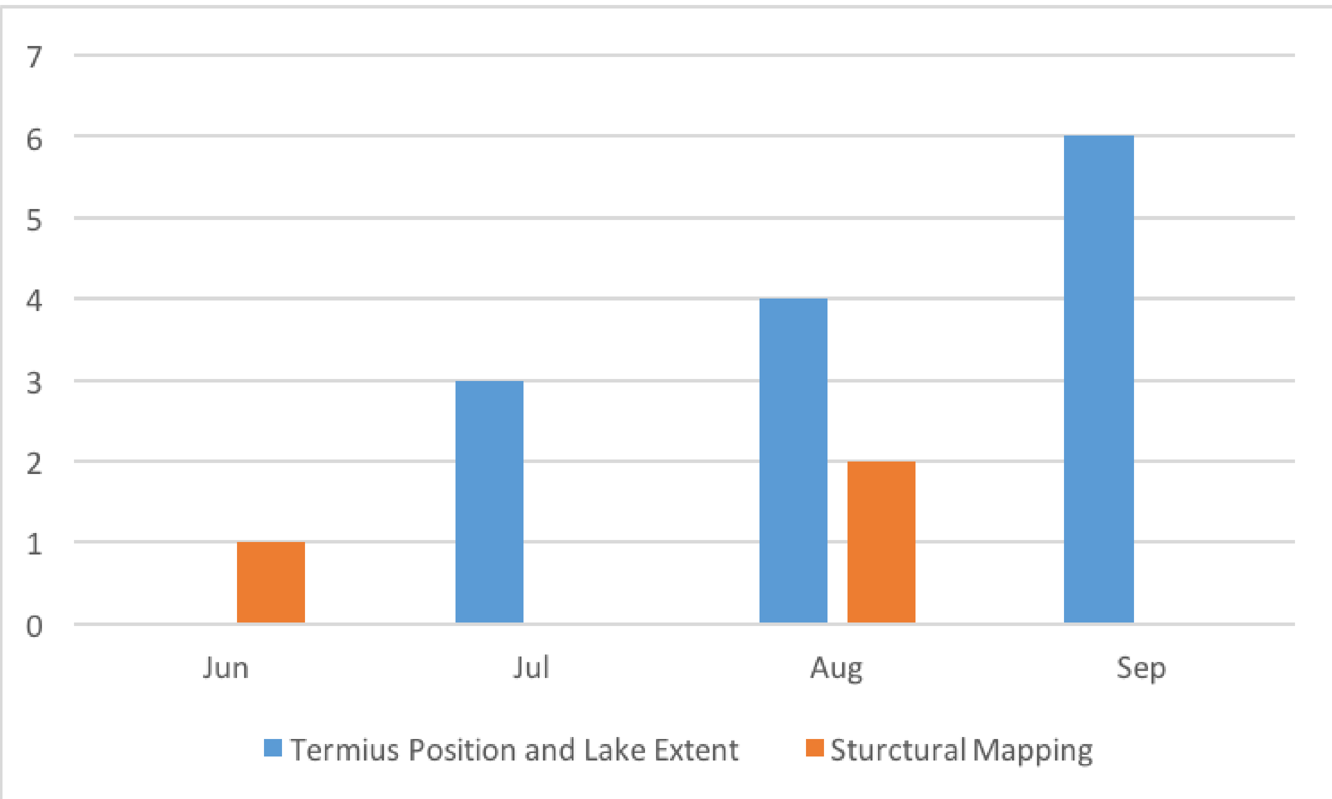

Fig. A.1. The number of images acquired in each month for terminus position and lake extent calculations and structural datasets.

ACKNOWLEDGEMENTS

We would like to thank Eyjólfur Magnússon for sharing with us his bedrock topography data for Fjallsjökull.